HHS Public Access

Author manuscript

*Neuron*. Author manuscript; available in PMC 2019 June 06.

Published in final edited form as:

*Neuron*. 2018 June 06; 98(5): 977–991.e5. doi:10.1016/j.neuron.2018.04.022.

# Excitatory and inhibitory neurons utilize different $Ca^{2+}$ sensors and sources to regulate spontaneous release

**Nicholas A. Courtney**, **Joseph S. Briguglio**, **Mazdak M. Bradberry**, **Christina Greer**, and **Edwin R. Chapman**[†]

Department of Neuroscience and Howard Hughes Medical Institute. University of Wisconsin-Madison, 1111 Highland Ave., Madison, WI 53705

## Summary

Spontaneous neurotransmitter release (mini) is an important form of $Ca^{2+}$-dependent synaptic transmission that occurs in the absence of action potentials. A molecular understanding of this process requires an identification of the underlying $Ca^{2+}$-sensors. Here, we address the roles of the relatively low- and high-affinity $Ca^{2+}$ sensors, synapotagmin-1 (syt1) and Doc2α/β, respectively. We found that both syt1 and Doc2 regulate minis but, surprisingly, their relative contributions depend on whether release was from excitatory or inhibitory neurons. Doc2α promoted glutamatergic minis, while Doc2β and syt1 both regulated GABAergic minis. We identified $Ca^{2+}$ ligand mutations in Doc2 that either disrupted or constitutively activated the regulation of minis. Finally, $Ca^{2+}$ entry via voltage-gated $Ca^{2+}$ channels triggered miniature GABA release by activating syt1, but had no effect on Doc2-driven minis. This work reveals an unexpected divergence in the regulation of spontaneous excitatory and inhibitory transmission in terms of both $Ca^{2+}$ sensors and sources.

## Introduction

Though evoked neurotransmitter release is the primary means of chemical communication between neurons, it is now clear that spontaneous release, occurring in the absence of action potentials, also plays a crucial role in synaptic structure and function. Spontaneous release modulates post-synaptic excitability by regulating the tonic activity of high-affinity receptors (Farrant and Nusser, 2005; Kombian et al., 2000), or by directly shaping action potentials (Carter and Regehr, 2002). Spontaneous release also suppresses post-synaptic protein synthesis (Sutton et al., 2004; Sutton and Schuman, 2006; Sutton et al., 2006), stabilizes

[†]Corresponding author: chapman@wisc.edu.



***Author Contributions:*** N.C. and E.R.C. designed the project and wrote the manuscript. N.C. conducted and analyzed the electrophysiology and the experiments in PC12 cells. N.C. also conducted the molecular biology work. J.B. performed the neuron imaging experiments and contributed to writing the corresponding sections. N.C. quantified these imaging experiments. M.B. designed and performed the biochemistry and presynaptic $Ca^{2+}$ imaging experiments, and contributed to writing the corresponding sections. J.B and C.G. conducted the RNAscope experiments.

***Declaration of Interests:*** The authors declare no competing interests.

dendritic spines (McKinney et al., 1999), maintains receptor density in the post-synapse (Ehlers et al., 2007), and mediates long-term forms of synaptic plasticity (Frank et al., 2006; Zhang et al., 2009). Despite the physiological importance of this mode of transmission, the molecular mechanisms that regulate spontaneous fusion, and how these mechanisms differ from evoked release, remain unclear (Ramirez and Kavalali, 2011).

The majority of spontaneous release events are $Ca^{2+}$-dependent (Groffen et al., 2010; Xu et al., 2009). Previous studies have identified two putative intracellular $Ca^{2+}$-sensors that facilitate miniature events (minis): synaptotagmin-1 (syt1) (Xu et al., 2009) and the cytosolic double C2-domain protein β (Doc2β) (Groffen et al., 2010). Syt1, Doc2β, and another closely-related Doc2 isoform, Doc2α,bind $Ca^{2+}$ and phospholipids via two tandem C2 domains; both Doc2 isoforms exhibit considerably slower membrane binding kinetics and higher affinities for $Ca^{2+}$ as compared to syt1 (Brose et al., 1992; Kojima et al., 1996; Groffen et al., 2006; Yao et al., 2011). The finding that syt1 functions as a $Ca^{2+}$-sensor for spontaneous neurotransmission was based on experiments using a supra-physiological range of extracellular $Ca^{2+}$ (up to 10 mM), without examining whether or how this low-affinity sensor regulates spontaneous release at physiologically-relevant [$Ca^{2+}$] (Xu et al., 2009). Furthermore, whether Doc2β is a direct $Ca^{2+}$-sensor or merely in the $Ca^{2+}$-sensing pathway is controversial. Namely, it was reported that a $Ca^{2+}$ ligand mutant form of Doc2β, that was unable to bind $Ca^{2+}$, was still able to rescue the decrease in mini frequency observed in Doc2β KO neurons (Pang et al., 2011). However, specific $Ca^{2+}$ ligand mutations in Doc2 have been reported to result in constitutive activation of the protein (Groffen et al., 2006; Xue et al., 2015). Whether this constitutive activity was present in the mutant utilized by Pang et al. (2011) was not examined. Thus, we reasoned that a thorough and direct comparison of wild type (WT) and mutant versions of these sensors would yield valuable insights into the mechanisms regulating $Ca^{2+}$-dependent spontaneous fusion.

Here, we recorded miniature events in Doc2α, Doc2β, and syt1 individual KO neurons, and unexpectedly observed that the roles played by each of these proteins depended on whether minis were glutamatergic or GABAergic. This segregation was due, in part, to differential expression of Doc2 isoforms, and to distinct differences in how voltage-gated $Ca^{2+}$ channels influence spontaneous release from GABAergic versus glutamatergic neurons. Separately, we demonstrate that both Doc2α and Doc2β must be capable of binding $Ca^{2+}$ to drive spontaneous fusion. We reconcile these results with published data (Pang et al., 2011) by showing that a mutant previously used to suggest a $Ca^{2+}$-independent role for Doc2β in spontaneous release is, instead, a gain-of-function mutation that mimics a $Ca^{2+}$-bound state. Indeed, expressing this mutant form of Doc2β in KO neurons renders the majority of spontaneous release events $Ca^{2+}$-independent. We conclude that Doc2α, Doc2β, and syt1 function as direct $Ca^{2+}$-sensors that drive spontaneous fusion, and their distinct contributions to this form of transmission represent an unanticipated divergence in the release machinery between GABAergic and glutamatergic neurons.

## Results

### Individual KO of Doc2α, Doc2β, and syt1 differentially affect spontaneous glutamate versus GABA release

To examine $Ca^{2+}$-dependent regulation of spontaneous glutamate release, pharmacologically-isolated AMPA receptor-mediated miniature excitatory post-synaptic currents (mEPSCs) were recorded from cultured mouse hippocampal neurons in the presence of TTX (1 μM). Separately, pharmacologically-isolated $GABA_A$ receptor-mediated miniature inhibitory post-synaptic currents (mIPSCs) were also recorded in the presence of TTX. Acute removal of free $Ca^{2+}$ via the application of BAPTA-AM (30 μM) and cyclopiazonic acid (CPA, 30 μM) in $Ca^{2+}$-free bath solution, which decreased the basal free [$Ca^{2+}$] in the presynaptic compartment from ~50 nM to ~30 nM (Supp. Fig. 1), reduced the frequency of mEPSCs by 87 ± 2% (n = 5; p = 0.003 paired t-test; Fig. 1A) and mIPSCs by 86 ± 4% (n = 4; p = 0.03 paired t-test; Fig. 1B). Thus, the majority of minis are regulated by $Ca^{2+}$ that presumably acts via $Ca^{2+}$-sensing proteins (Groffen et al., 2010; Xu et al., 2009).

To determine the roles of the $Ca^{2+}$ sensors Doc2α, Doc2β, and syt1, we recorded from hippocampal mouse neurons lacking each of these proteins; WT littermates served as controls. Syt1 KO neurons exhibited a ~3-fold increase in the frequency of both mEPSCs and mIPSCs, consistent with syt1's previously reported function as an inhibitory clamp of spontaneous fusion (mEPSCs: syt1 WT: 2.8 ± 0.5 Hz, n = 16; syt1 KO: 9.7 ± 1.2 Hz, n = 18, p < 0.001; mIPSCs: syt1 WT: 1.0 ± 0.2 Hz, n = 14; syt1 KO: 3.1 ± 0.6 Hz, n = 10; p < 0.001; Fig. 1C, D) (Broadie et al., 1994; Chicka et al., 2008, but see Liu et al., 2009; Wierda and Sørensen, 2014). Loss of each of the two $Ca^{2+}$ sensitive Doc2 isoforms, α and β, had differential effects on mEPSC and mIPSC frequencies. In Doc2α KO neurons, the frequency of glutamatergic mEPSCs was reduced by 56% (Doc2α WT: 3.5 ± 0.6 Hz, n = 17; Doc2α KO: 1.6 ± 0.3 Hz, n = 20; p = 0.002; Fig. 1C) while GABAergic mIPSCs were unchanged (Doc2α WT: 0.9 ± 0.2 Hz, n = 13; Doc2α KO: 1.1 ± 0.2 Hz, n = 11; p = 0.63; Fig. 1D). In contrast, Doc2β KO neurons had normal mEPSC frequencies (Doc2β WT: 3.1 ± 0.5 Hz, n = 19; Doc2β KO: 3.5 ± 0.5 Hz, n = 16; p = 0.57; Fig. 1C) but had ~60% fewer mIPSCs (Doc2β WT: 1.0 ± 0.2 Hz, n = 15; Doc2β KO: 0.4 ± 0.1 Hz, n = 16; p = 0.003; Fig. 1D). In all cases, the loss of each respective $Ca^{2+}$ sensor did not affect the amplitude or shape of mEPSCs or mIPSCs, or the density of excitatory or inhibitory synapses (Supp. Fig. 2). As previous reports have shown that KO of Doc2α and/or β does not alter synchronous release or the size of the readily-releasable pool in neurons (Groffen et al., 2010; Yao et al., 2011), these changes in mini frequencies are unlikely to be secondary to defects in vesicle docking/priming or due to deficiencies in synchronous release.

The observation that Doc2α regulates spontaneous glutamate release, while Doc2β regulates spontaneous GABA release, reveals an unexpected difference between excitatory and inhibitory neurons. In contrast, syt1 clamped both mIPSCs and mEPSCs. Whether syt1 also drives minis in response to $Ca^{2+}$ (Xu et al., 2009), in either excitatory or inhibitory neurons, is addressed in the following section.

## Loss of syt1 alters the $Ca^{2+}$-dependence of spontaneous GABA, but not glutamate, release at physiologically relevant $Ca^{2+}$ concentrations

We next examined how the loss of either Doc2α or syt1 altered the $Ca^{2+}$-dependence of glutamatergic mEPSC frequency over a physiological range of extracellular $Ca^{2+}$ ($[Ca^{2+}]_O$), estimated to be ~1–2 mM for the mammalian brain (Jones and Keep, 1988). In WT neurons, increasing $[Ca^{2+}]_O$ from 1.2 mM to 2.4 mM consistently increased the frequency of mEPSCs by ~25% (syt1 WT: 26 ± 6%, n = 11, p = 0.002 paired t-test; Doc2α WT: 20 ± 10%, n = 10, p = 0.028 paired t-test; syt1 WT vs. Doc2α WT: p = 0.61; Fig. 2A–C). This $Ca^{2+}$-induced increase in mini frequency was unaffected by loss of syt1 (1.2 vs 2.4 mM $Ca^{2+}$, syt1 KO: 25 ± 7% increase, n = 12, p = 0.037 paired t-test; p = 0.85 vs. syt1 WT; Fig. 2A–C). We note that a prior report concluding that syt1 does trigger mEPSCs used a non-physiological range of $[Ca^{2+}]_O$ that extended up to 10 mM (Xu et al., 2009). Indeed, we find that increasing $[Ca^{2+}]_O$ from 1.2 to 10.0 mM, mimicking the experimental conditions of Xu et al., 2009, revealed a significant increase in syt1 regulated mEPSCs (Supp. Fig. 3A, B). Thus, our data suggest that while syt1 facilitates spontaneous glutamate release at elevated $[Ca^{2+}]_O$, its contribution is likely to be minimal at physiologically relevant $[Ca^{2+}]_O$. To control for a possible confound due to the 'unclamped' phenotype of syt1 KO neurons, we also examined syt1 KO neurons that virally expressed either wildtype syt1 (syt1 WT) or a calcium-ligand mutant form (syt1 CLM; D363,365N) that partially clamps mini frequencies (Supp. Fig. 3C, D), but cannot rescue $Ca^{2+}$-dependent evoked release in KO neurons (Nishiki and Augustine, 2004). In agreement with the results above, we observed a similar $Ca^{2+}$-induced increase in mEPSC frequency (from 1.2 to 2.4 mM $[Ca^{2+}]_O$) in KO neurons expressing either syt1 WT or syt1 CLM. These data again suggest that $Ca^{2+}$ binding by syt1 does not promote mEPSCs over a physiological range of $[Ca^{2+}]_O$ (Supp. Fig. 3E). In contrast, loss of Doc2α abolished $Ca^{2+}$-induced promotion of mEPSC frequency in the physiological range of $[Ca^{2+}]_O$, as increasing $[Ca^{2+}]_O$ from 1.2 mM to 2.4 mM resulted in no significant change in the frequency of mEPSCs in the KO (1.2 vs 2.4 mM $Ca^{2+}$, Doc2α KO: 6 ± 7% decrease, n = 12, p = 0.48 paired t-test; Doc2α KO vs. Doc2α WT: p = 0.045; Fig. 2A–C). Together, these data suggest that at physiological $[Ca^{2+}]_O$, Doc2α, but not syt1, promotes $Ca^{2+}$-dependent spontaneous release in glutamatergic neurons.

Next, we determined how the loss of Doc2β or syt1 altered $Ca^{2+}$-dependent mIPSC frequencies at physiological $[Ca^{2+}]_O$. Increasing $[Ca^{2+}]_O$ from 1.2 mM to 2.4 mM in WT littermates from each mouse line consistently increased the frequency of mIPSCs by ~20% (syt1 WT: 21 ± 5%, n = 11, p = 0.007 paired t-test; Doc2β WT: 17 ± 4%, n = 11, p = 0.004 paired t-test; syt1 WT vs. Doc2β WT: p = 0.60; Fig. 2D–F). Surprisingly, both Doc2β and syt1 were required for this $Ca^{2+}$-dependent increase in mIPSC frequency. Loss of Doc2β significantly reduced, but did not abolish, $Ca^{2+}$-dependent spontaneous GABA release. Syt1 KOs exhibited a similar effect on mIPSCs (1.2 vs 2.4 mM $Ca^{2+}$; syt1 KO: 7 ± 3% increase, n = 9, p = 0.014 paired t-test; p = 0.037 vs. syt1 WT; Doc2β KO: 5 ± 3% increase, n = 10, p = 0.024 paired t-test; p = 0.031 vs. Doc2β WT; Fig. 2D–F). Syt1 KO neurons expressing syt1 CLM also had an impaired $Ca^{2+}$-induced increase in mIPSC frequency when compared against syt1 KO neurons expressing syt1 WT (Supp. Fig. 3C, D, F), further suggesting that $Ca^{2+}$ binding by syt1 is an important driver of mIPSCs. Thus, at physiologically relevant $[Ca^{2+}]_O$, both syt1 and Doc2β facilitate miniature GABA release in response to $Ca^{2+}$.

### $Ca^{2+}$-insensitive, loss-of-function Doc2 mutants fail to support spontaneous release

It was previously reported that Doc2β, though a necessary component of the $Ca^{2+}$-sensing pathway, does not need to directly bind $Ca^{2+}$ to promote spontaneous release and thus is not a $Ca^{2+}$-sensor for this form of exocytosis (Pang et al., 2011). The pivotal experiment leading to this conclusion examined a mutant form of Doc2β in which six of the $Ca^{2+}$-coordinating acidic residues (three in each C2-domain) were substituted with alanines to abolish $Ca^{2+}$ binding activity (here termed Doc2β-6x, Fig. 3B); these mutations include substitution of D220 in C2A. Importantly, it is well established that substitution of D220, either alone (Xue et al., 2015) or in combination with additional substitutions of other $Ca^{2+}$-coordinating residues (Gaffaney et al., 2014; Groffen et al., 2006), confers new functions and constitutive activity to Doc2β in terms of membrane binding and asynchronous release. Whether this D220 mutation confers constitutive activity regarding the regulation of spontaneous release, alone or in the context of the Doc2β-6x mutant (Pang et al., 2011), has not been examined. We address this question below.

Upon binding $Ca^{2+}$, Doc2α and β translocate to the plasma membrane (Groffen et al., 2004). Thus, translocation assays are widely utilized to characterize how mutations affect $Ca^{2+}$-dependent membrane binding in native cellular environments. Here, WT and mutant versions of Doc2α and β were tagged with GFP at the C-terminus and expressed in PC12 cells to visualize their subcellular distributions (Fig. 3A, B) (Gaffaney et al., 2014; Groffen et al., 2006). PC12 cells were used because presynaptic boutons are too small to monitor translocation. Both Doc2α-WT and Doc2β-WT localized primarily to the cytosol under control conditions (Doc2α-WT: 0.79 ± 0.04 PM/cyto, n = 12; Doc2β-WT: 0.83 ± 0.04 PM/cyto, n = 8, Fig. 3C–E), as quantified by the ratio of the average GFP fluorescent intensity at the plasma membrane (PM), divided by the average intensity across the cytosol (termed PM/cyto, see Fig. 3 and Methods). As expected, both isoforms translocated to the plasma membrane upon treatment with ionomycin (ctrl vs. 15 μM iono; Doc2α-WT: 1.88 ± 0.28 PM/cyto, n = 12, p = 0.001 paired t-test; Doc2β-WT: 2.22 ± 0.47 PM/cyto, n = 8, p = 0.002 paired t-test; Fig. 3C–E). Consistent with previous reports (Xue et al., 2015), substitution of an asparagine for the $Ca^{2+}$-coordinating residue D303 in Doc2β (Doc2β-D303N) completely disrupted $Ca^{2+}$-dependent translocation (ctrl: 0.83 ± 0.04 PM/cyto, iono: 0.92 ± 0.07 PM/cyto, n = 8, p = 0.17 paired t-test, Fig. 3). An analogous mutation to Doc2α (Doc2α-D291N) had the same disruptive effect (ctrl: 0.87 ± 0.04 PM/cyto, iono: 0.93 ± 0.05 PM/cyto, n = 9, p = 0.27 paired t-test, Fig. 3). In sharp contrast to these loss-of-function mutants, we found that the Doc2β-6x mutant (Pang et al., 2011) was constitutively localized to the PM under basal, unstimulated conditions (ctrl: 1.64 ± 0.05 PM/cyto, n = 11, $p < 0.001$ vs. Doc2β-WT in Ctrl conditions, Fig. 3), and did not further translocate in ionomycin (iono: 1.56 ± 0.06, n = 11, p = 0.11 vs. ctrl). It was proposed that the gain-of-function exhibited by a similar set of $Ca^{2+}$ ligand mutations in Doc2β (D218,220N) was the result of an increase in $Ca^{2+}$-affinity, rather than true $Ca^{2+}$-independent activity (Groffen et al., 2006). However, as this 6X mutant was reported to not bind $Ca^{2+}$ at all (Pang et al., 2011), it likely mimics the $Ca^{2+}$-bound state.

We next expressed the untagged versions of these constructs in Doc2α or β KO neurons using lentivirus (Supp. Fig. 4) and tested whether they could rescue the mini frequency

phenotypes. In Doc2α KO neurons (Fig. 4A), expressing Doc2α-WT rescued the frequency of mEPSCs compared to GFP-expressing controls (GFP: 1.7 ± 0.3 Hz, n = 27; WT Doc2α: 3.7 ± 0.5 Hz, n = 37; $p < 0.001$; Fig. 4B). However, the $Ca^{2+}$-ligand mutant Doc2α-D291N failed to rescue mEPSC frequency (Doc2α-D291N: 1.7 ± 0.2 Hz, n = 32; p = 0.99 vs. GFP; Fig. 4B). Similarly, rescue of Doc2β KO neurons (Fig. 4C) with Doc2β-WT restored mIPSC frequency (GFP: 0.4 ± 0.1 Hz, n = 11; WT Doc2β: 1.4 ± 0.2 Hz, n = 11; $p < 0.001$; Fig. 4D) while expression of Doc2β-D303N failed to restore mIPSC frequency (Doc2β-D303N: 0.5 ± 0.1 Hz, n = 9; p = 0.35 vs. GFP; Fig. 4D). Thus, we conclude that Doc2α and β must interact with $Ca^{2+}$ to drive miniature release. This strongly implicates both isoforms as direct $Ca^{2+}$-sensors for spontaneous neurotransmission.

Finally, when Doc2β-6x was expressed in Doc2β KO neurons, mIPSCs were significantly more frequent than in Doc2β-WT expressing KO neurons (Doc2β-6x: 2.2 ± 0.2 Hz, n = 11; $p < 0.001$ vs. GFP; p = 0.002 vs. WT Doc2β; Fig. 4D). Furthermore, Doc2β-6x yielded mIPSCs that were largely independent of $Ca^{2+}$ (30 μM BAPTA-AM and 30 μM CPA in $Ca^{2+}$-free bath) (Doc2β-WT, $Ca^{2+}$-free: 0.1 ± 0.1 Hz, n = 5; Doc2β-6x, $Ca^{2+}$-free: 1.4 ± 0.2 Hz, n = 6; $p < 0.001$; Fig. 4E). Roughly a third of these events were still $Ca^{2+}$-sensitive, and were likely mediated by a distinct sensor (i.e., syt1 and perhaps other proteins such as the $Ca^{2+}$-sensing GPCR (Vyleta and Smith, 2011)). These data, in agreement with the translocation data above, are consistent with the interpretation that the Doc2β-6x mutant is a gain-of-function variant that constitutively mimics the $Ca^{2+}$-bound state of WT Doc2β.

## Doc2α and β are functionally redundant, differentially expressed, and localized to synaptic boutons

The observed neuronal subtype-specific mini phenotypes could result from differential expression patterns of Doc2α vs. β or differences in their respective biochemical properties. Thus, we separately expressed either WT Doc2α or WT Doc2β under pan-neuronal promoters in Doc2α single KO neurons to determine whether rescue of mEPSC frequency was isoform specific. Above, we demonstrated that WT Doc2α rescued the reduced frequency of mEPSCs observed in Doc2α KO neurons (Fig. 4). In parallel experiments, we found that WT Doc2β also rescued mEPSC frequency in Doc2α KO neurons (WT Doc2β: 2.9 ± 0.4 Hz, n = 16, ANOVA p = 0.002, p = 0.019 vs GFP, p = 0.29 vs. WT Doc2α; Fig. 5A). Similar experiments in Doc2β single KO neurons revealed that expression of either Doc2α or Doc2β equally rescued mIPSC frequency (WT Doc2α: 1.7 ± 0.2 Hz, n = 12, ANOVA $p < 0.001$, $p < 0.001$ vs. GFP, p = 0.26 vs. WT Doc2β; Fig. 5B).

Because exogenous expression of either isoform could rescue the single KO phenotype, it is likely that Doc2α and β are differentially expressed in glutamatergic versus GABAergic neurons. However, we have been unable to identify antibodies that can accurately label and differentiate endogenous Doc2α and Doc2β when controlled against single and double KO neurons (unpublished data). Therefore, we used RNAScope technology to examine the expression patterns of Doc2α and β mRNA in brain slices (10 μm thick, coronal) obtained from adult WT mice. We first examined the stratum pyramidale in the CA3 region of the hippocampus (Fig. 5C, top). This brain region is densely populated by glutamatergic pyramidal neurons; we observed very few GABAergic interneurons (visualized by VGAT

mRNA staining; Fig. 5C, middle) and those interneurons tended to be located just outside of the stratum pyramidale. In agreement with our functional data, we found that glutamatergic pyramidal neurons strongly expressed Doc2α-mRNA; Doc2β-mRNA puncta were occasionally, but rarely, detected (Fig. 5C middle and bottom). Next, to better observe the expression pattern of Doc2 isoforms in GABAergic neurons, we examined brain sections containing the dorsal striatum (Fig. 5D, top). The dorsal striatum is densely populated by GABAergic neurons (> 95% of total neurons; Fig 5D, middle) and is known to lack glutamatergic neurons altogether. Striatal GABAergic neurons strongly expressed Doc2β-mRNA while Doc2α-mRNA was largely absent (Fig. 5D, middle and bottom); we observed that <10% of neurons (7 out of 94) were positive for both Doc2 isoforms and that no striatal neurons only express Doc2α. Together, these data demonstrate that Doc2 isoforms are differentially expressed in excitatory and inhibitory neurons in these two regions of the adult mouse brain.

Due to technical limitations, the subcellular distribution of Doc2 protein in neurons remains an open question. The only evidence for synaptic localization stems from subcellular fractionation assays (Verhage et al., 1997), where Doc2 was present in the synaptosomal plasma membrane and synaptic vesicle fractions. To localize Doc2 in living neurons, we generated C-terminal HaloTag fusion proteins of Doc2 isoforms (Fig. 6A, B). For imaging experiments, the HaloTag fusion proteins were conjugated with JF646 HaloTag ligand dye (Supp. Fig. 5). Synaptic boutons were identified by transfection of mRuby-tagged synaptophysin. As cytosolic proteins, Doc2 fusion proteins were initially indistinguishable from volumetric markers, like monomeric GFP, that fill the cytosol when highly expressed in neurons (Supp. Fig. 6A). So, we infected Doc2 KO hippocampal cultures with smaller lentiviral titers of the Doc2 HaloTag fusion constructs (Supp. Fig. 6A). In these experiments, we observed a quantifiable enrichment of both Doc2α-HaloTag and Doc2β-HaloTag in many, though not all, of the synaptic boutons in the cognate KO neurons (Doc2α: enriched in 24 ± 4% of boutons, n = 5 fields of view / 3 pups, p = 0.024 vs. GFP; Doc2β: enriched in 24 ± 5% of boutons, n = 6 fields of view / 3 pups, p = 0.012 vs GFP; Figure 6C, D). Importantly, cytosolic GFP that was co-infected alongside the Doc2-HaloTag fusion proteins was not similarly enriched at synapses when using lower viral titers (Fig. 6C, D), and the Doc2-HaloTag signals (at low expression levels) were clearly above the background signal (Supp. Fig. 5). Furthermore, the lower viral titers of both HaloTag fusion proteins fully rescued spontaneous release in corresponding KO neurons (Supp. Fig. 6B, C), indicating that these proteins are functional at this expression level and that the HaloTag did not disrupt function or localization. Together, these observations indicate that Doc2α and Doc2β are enriched in synaptic boutons in living neurons.

## Doc2β mutant phenotypes were correlated with alterations in $Ca^{2+}$-dependent membrane binding

As with syt1, Doc2 exhibits $Ca^{2+}$-dependent and -independent interactions with t-SNAREs and membranes (Kojima et al., 1996; Friedrich et al., 2008; Yao et al., 2011). We employed biochemical approaches to evaluate the impact of the Doc2β D303N and 6x mutations on these interactions. We first examined membrane-binding activity using co-sedimentation assays (Fig. 7A). In the absence of $Ca^{2+}$, increasing the mole fraction of

phosphatidylinositol 4,5-bisphosphate ($PIP_2$) and phosphatidylserine (PS) caused a dose-dependent increase in membrane binding for syt1, Doc2β, and Doc2β-D303N (Fig. 7B, C). This effect was strongly synergistic, as both $PIP_2$ and PS together were required for significant $Ca^{2+}$-independent binding activity (Fig. 7C). In contrast, $Ca^{2+}$-independent lipid binding of Doc2β-6x was relatively strong in the presence of either $PIP_2$ or PS; again, a combination of these lipids exerted an additive effect on binding (Fig. 7C). Saturating levels of $Ca^{2+}$ (0.5 mM) enhanced the binding of Doc2β-WT and D303N to each lipid mixture tested (Fig. 7B, C). The 6x mutant bound more weakly in the presence of $Ca^{2+}$, perhaps due to charge shielding by $Ca^{2+}$.

While Doc2β-WT and D303N appeared to bind membranes equally well at saturating $[Ca^{2+}]$, a $Ca^{2+}$ titration with liposomes containing 1% $PIP_2$ revealed a 3-fold increase in the apparent $[Ca^{2+}]_{1/2}$ for the mutant (WT: 47.3 ± 5.1 nM; D303N: 148 ± 12 nM; $p < 0.001$; Fig. 7D). The D303N mutation also significantly affected the Hill slope of the $Ca^{2+}$ curve (WT: 1.49 ± 0.16; D303N: 2.30 ± 0.38, Fig. 7D). Binding of the 6x construct under these conditions was not measured, as it is entirely membrane-bound in the $Ca^{2+}$-free state under these conditions (Fig. 7B, C).

We next compared the t-SNARE-binding activities of the syt1 and Doc2β constructs using a HaloTag-based pulldown assay (Fig. 7E). Purified HaloTag-C2AB fusion constructs were covalently linked to chloroalkane-bearing beads and used to pull down the t-SNARE heterodimer. Consistent with prior studies, this assay produced robust $Ca^{2+}$-independent interactions between t-SNARE heterodimers and either syt1 or WT-Doc2β, and these interactions were enhanced by the presence of $Ca^{2+}$ (EGTA vs. $Ca^{2+}$; syt1: $n = 5$, $p = 0.002$; Doc2β: $n = 5$, $p < 0.001$; Fig. 7F, G). The D303N construct failed to exhibit a $Ca^{2+}$-dependent increase in t-SNARE binding ($n = 5$, $p = 0.52$; Fig. 7G). As expected, the 6x construct also showed no $Ca^{2+}$-dependent enhancement of t-SNARE binding ($n = 5$, $p = 0.66$; Fig. 7G). However, in contrast to its constitutive activity in cells, this 6x mutation did not enhance $Ca^{2+}$-independent t-SNARE binding ($n = 5$; 6x EGTA vs. WT EGTA: $p = 0.89$; 6x EGTA vs. WT $Ca^{2+}$: $p < 0.001$). Thus, t-SNARE binding, when both $Ca^{2+}$-dependent and -independent interactions are considered, did not correlate with the spontaneous release phenotype (Fig. 5). These results suggest that while the D303N and 6x mutations may alter SNARE binding activity, changes in this interaction are not predictive of the ability of each construct to regulate spontaneous fusion.

## Voltage-gated calcium channels (VGCCs) are a $Ca^{2+}$-source for syt1, but not Doc2, regulated mIPSCs

In the final set of experiments, we sought to understand why syt1 facilitated mIPSCs, but not mEPSCs, at physiologically relevant $[Ca^{2+}]_O$. A recent study reported that blocking $Ca^{2+}$ influx through VGCCs inhibited spontaneous GABA but not spontaneous glutamate release (Tsintsadze et al., 2017). As the $Ca^{2+}$-affinity of syt1 is considerably lower than Doc2, and VGCCs can be a source of relatively high $[Ca^{2+}]$ signaling, we explored whether there might be a mechanistic relationship between mIPSCs promoted by the activity of both syt1 and VGCCs. We found that fully blocking VGCCs with saturating cadmium ($Cd^{2+}$, 200 μM) in WT neurons resulted in a ~33% inhibition of mIPSCs (ctrl: 1.1 ± .3 Hz, $Cd^{2+}$: 0.7 ± 0.2 Hz,

n = 5, p = 0.039, paired t-test; Fig. 8A) but had no effect on the frequency of mEPSCs (ctrl: 3.7 ± 0.6 Hz, $Cd^{2+}$: 3.9 ± 0.6 Hz, n = 4, p = 0.53, paired t-test, Fig. 8A). We repeated this experiment measuring mIPSCs in single KO neurons and found that loss of Doc2β increased the sensitivity to $Cd^{2+}$, resulting in a 63 ± 8% reduction in mIPSC frequency (ctrl: 0.5 ± 0.1 Hz, $Cd^{2+}$: 0.2 ± 0.1 Hz, n = 5, p = 0.002, paired t-test; Fig. 8B–D) while loss of syt1 abolished this sensitivity altogether (ctrl: 3.1 ± 0.1 Hz, $Cd^{2+}$: 3.0 ± 0.1 Hz, n = 4, p = 0.24, paired t-test; Fig. 8B–D). These data indicate that $Ca^{2+}$ influx through VGCCs selectively activates syt1 to drive spontaneous GABA release. The increase in $Cd^{2+}$ sensitivity observed in Doc2β KO neurons is likely attributable to a greater percentage of miniature events being driven by syt1 when Doc2β is absent. We conclude that $Ca^{2+}$ entry through spontaneously opening VGCCs can activate syt1 to drive miniature release of GABA, but not glutamate (Fig. 8E). These results identify syt1 and its relationship to VGCCs as a key point of divergence in GABA and glutamate neurons.

## Discussion

In this study, we compared the roles of the $Ca^{2+}$-sensing proteins syt1 and Doc2α/β in regulating $Ca^{2+}$-dependent, action potential independent, spontaneous neurotransmitter release. Syt1 is a low-affinity $Ca^{2+}$-sensor that couples action-potential induced $Ca^{2+}$-entry to synchronous neurotransmitter release in both excitatory and inhibitory neurons (Chapman, 2008). While a previous report concluded that syt1 is also a major $Ca^{2+}$-sensor for spontaneous release in both glutamatergic and GABAergic neurons (Xu et al., 2009), it is important to note that this conclusion was drawn from experiments conducted over a supra-physiological range of $[Ca2+]_O$ (up to 10 mM). Here we show that when experiments are limited to near-physiological $[Ca^{2+}]_O$, syt1 promotes $Ca^{2+}$-dependent minis in inhibitory, but not excitatory, neurons. In inhibitory neurons, we found that $Ca^{2+}$ influx through VGCCs was sufficient to activate syt1 and drive spontaneous release. This $Ca^{2+}$ influx may arise from the spontaneous opening of a single VGCC, which is sufficient to drive quantal release in some cases (Bucurenciu et al., 2010; Shahrezaei et al., 2006; Stanley, 1993), or from the coordinated, yet still spontaneous, opening of several channels (Williams et al., 2012). Therefore, we speculate that one-third of mIPSCs (i.e., the percentage sensitive to $Cd^{2+}$) are triggered by syt1, potentially via mechanisms similar to those mediating action potential dependent release. However unlike syt1-dependent evoked release, which displays strong $Ca^{2+}$ cooperativity, doubling $[Ca^{2+}]_O$ had only a minor effect on mIPSC frequency, consistent with previous observations (Williams et al., 2012). We note that only a fraction of total events are syt1 dependent (~30%) and the degree of cooperativity between $[Ca^{2+}]_O$ and syt1-independent spontaneous fusion events (i.e. the majority of mIPSCs) is unclear. Furthermore, it is unlikely that the $[Ca^{2+}]$ profiles seen by syt1 during spontaneous and evoked release would be similar. Differences in these $[Ca^{2+}]$ profiles may arise due to differences in the number of activated VGCCs during each distinct event (i.e. spontaneous VGCC opening versus action potential driven VGCC opening). Additionally, evoked and spontaneous release may occur at distinct sites within an active zone (Reese and Kavalali, 2016). Different coupling distances between VGCCs and syt1, stemming from distinct release sites, would also cause differences in the corresponding $[Ca^{2+}]$ profiles. Why VGCCs acting via syt1 did not influence mEPSCs from glutamatergic neurons – or at least

why supra-physiological $[Ca^{2+}]_O$ was required for syt1 to contribute to mEPSC frequency (Supp. Fig. 3) – remains unclear. One potential explanation is that GABAergic terminals, in both hippocampal cultures and slices, have been reported to be more responsive to $Ca^{2+}$ and have larger depolarization-induced $Ca^{2+}$ influx than glutamatergic terminals (Verderio et al., 2004). Thus, in glutamatergic neurons, the spontaneous opening of a single or even multiple VGCCs may not sufficiently elevate local $[Ca^{2+}]$ to activate the relatively low-affinity sensor, syt1. Finally, loss of syt1 resulted in an 'unclamped' phenotype in both inhibitory and excitatory neurons with the rate of minis increasing by ~3-fold in both cases. These findings are consistent with syt1 being present on both glutamatergic and GABAergic synaptic vesicles. We also note that previous reports revealed that the clamping function of syt1 can be affected by non-cell-autonomous mechanisms; the molecular basis for this latter observation remain unclear (Liu et al., 2009; Wierda and Sørensen, 2014). The finding that syt1 drives only mIPSCs and not mEPSC, but clamps both forms of spontaneous release, further demonstrates that protein has distinct, separate roles in limiting and promoting fusion (Liu et al., 2014; Bai et al., 2016).

In contrast to the dual functionality of syt1, Doc2 acts only as a positive regulator of spontaneous fusion. Surprisingly, we observed a difference in the regulation of excitatory and inhibitory minis: Doc2α regulated mEPSCs while Doc2β regulated mIPSCs. This apparent difference in the function of each isoform was not due to biochemical differences, because pan-neuronal expression of either isoform was sufficient to rescue spontaneous release in both excitatory and inhibitory neurons. While these data directly contradict a previous report that rescue of spontaneous frequency in Doc2α/β double knockdown neurons was isoform dependent (Pang et al., 2011), they are in agreement with the observation that exogenous Doc2β expression rescued glutamatergic mini frequency in Doc2α/β double KO neurons (Groffen et al., 2010). Furthermore, our RNAScope experiments found that glutamatergic pyramidal neurons in the CA3 region of the hippocampus predominately expressed Doc2α-mRNA while GABAergic neurons in the striatum predominately expressed Doc2β-mRNA. This is consistent with a previous study examining the expression of Doc2α and β mRNA at the regional level of the rodent brain, which reported that Doc2β was the predominant isoform in brain regions that are primarily comprised of inhibitory neurons, such as the cerebellum and striatum, while Doc2α appeared to be the major isoform in the deeper layers of the cortex and the CA1/CA3 pyramidal layer of the hippocampus (Verhage et al., 1997). Thus, the subtype-specific phenotypes observed in our electrophysiological experiments can be explained by differences in expression of Doc2 isoforms between excitatory and inhibitory neurons. Furthermore, the fact that differential expression was observed in brain slices from adult mice makes it likely that our functional data and conclusions, obtained from cultured neurons, translate into a better understanding of an intact nervous system. Why separate isoforms of Doc2 evolved to differentially regulate spontaneous release in discrete populations of neurons, however, remains an open question.

It is controversial whether Doc2 is a direct $Ca^{2+}$-sensor for miniature release (Groffen et al., 2010) or instead is merely a component of the $Ca^{2+}$-sensing pathway without itself needing to bind $Ca^{2+}$ (Pang et al., 2011). We believe that the current study resolves this controversy by demonstrating two key points: 1) that loss-of-function $Ca^{2+}$-ligand mutants of Doc2 are

unable to support spontaneous fusion and 2) that other $Ca^{2+}$-ligand mutations, such as the one employed by Pang et al. (2011), cause a constitutive gain-of-function that activates Doc2 independent of $Ca^{2+}$ and drive $Ca^{2+}$-independent minis when expressed in neurons. These findings suggest that Doc2 directly binds $Ca^{2+}$ to regulate minis. The fact that constitutively activated Doc2 (i.e. Doc2β-6x) drives substantial mini frequencies in the complete absence of $Ca^{2+}$ further supports the conclusion that Doc2 is a direct and immediate $Ca^{2+}$-sensor for spontaneous fusion; activating Doc2 by itself is sufficient to drive minis in the absence of any other form of $Ca^{2+}$-signaling. Moreover, we demonstrate, for the first time, that Doc2 is indeed enriched in synaptic boutons in living neurons, where it could directly regulate the fusion machinery. These results suggest that Doc2 is either sorted to or retained in synapses by an unknown mechanism. Synaptic enrichment of Doc2 may be simply explained by its ability to associate with the synaptic vesicle fusion machinery; however, Doc2 does not appear to be uniformly distributed across all synapses. This heterogeneous distribution leads to an intriguing hypothesis that spontaneous transmission from individual boutons may be additionally regulated by the degree of Doc2 enrichment at that bouton. This hypothesis fits emerging models that the propensity of individual synaptic boutons to participate in spontaneous release varies greatly among different axonal terminals (Reese and Kavalali, 2016).

Having demonstrated that Doc2 is enriched in synapses, we turned to biochemical approaches to gain insights into its mechanism of action. Utilizing the loss-of-function mutant Doc2β-D303N and the constitutively active mutant Doc2β-6x, we found that the ability to associate with membranes best correlated with the ability of each mutant to regulate minis. The D303N mutant had impaired $Ca^{2+}$-dependent membrane interactions and did not support minis, while the 6X mutant was constitutively associated with membranes in reconstituted biochemical assays and in cells and constitutively drove minis in the absence of $Ca^{2+}$. We note a slight discrepancy between the biochemical and cell-based membrane interaction experiments using the D303N mutant. In response to $Ca^{2+}$, this mutant failed to translocate to the plasma membrane in cells but was still able to bind reconstituted membranes *in vitro*, albeit at a lower $Ca^{2+}$-affinity. We postulate that the C2A domain, unaltered in the D303N mutant, can still bind $Ca^{2+}$ and associate with membranes in biochemical assays, but for reasons that remain unclear this domain cannot drive efficient membrane association in native cell membranes. It is important to note that $Ca^{2+}$-binding specifically to the C2B domain, containing D303, is thought to be the crucial determinant for other cellular functions of Doc2 (Gaffaney et al., 2014; Xue et al., 2015), while $Ca^{2+}$-binding by C2A appears to be somewhat dispensable (Giladi et al., 2013; Xue et al., 2015). In short, Doc2 interactions with the plasma membrane, driven by $Ca^{2+}$ binding to C2B, is a crucial step in the regulation of miniature release. In contrast to membrane binding, $Ca^{2+}$-triggered t-SNARE binding activity was a poor predictor of whether the D303N or 6X mutant functioned during minis. No correlation was observed between the abilities of these mutants to bind t-SNAREs and to drive spontaneous release. This observation is consistent with reports that in some syt1 variants, $Ca^{2+}$-triggered SNARE binding activity did not coincide with the ability of these mutants to regulate fusion (Liu et al., 2014; Bai et al., 2016). At present, the relevance of syt1-t-SNARE interactions remains unresolved (Bhalla et al., 2006; Tucker et al., 2004; Zhou et al., 2015; Guan et al., 2017; Zhou et al., 2017).

Unlike syt1, Doc2 did not to respond to $Ca^{2+}$-influx from VGCCs: mEPSCs in general, and mIPSCs in syt1 KO neurons, were unaffected by $Cd^{2+}$. As Doc2α and β are orders of magnitude more sensitive to $Ca^{2+}$ than syt1 (Brose et al., 1992; Kojima et al., 1996; Groffen et al., 2006; Gaffaney et al., 2014), and have markedly slower intrinsic kinetics (Yao et al., 2011), these data support the hypothesis that Doc2 and syt1 translate distinct $Ca^{2+}$ signals, perhaps at distinct physical release sites, into spontaneous neurotransmission. We note similarities in our measurements for resting [$Ca^{2+}$] in the presynaptic compartment (~50 nM, Supp. Fig. 1) and the $[Ca^{2+}]_{1/2}$ of *in vitro* Doc2-lipid interactions (~50 nM, Fig. 7D), suggesting that basal cytosolic [$Ca^{2+}$] may potentially be a source for Doc2 activation. A number of additional $Ca^{2+}$ sources have been proposed to contribute to spontaneous fusion, including: $Ca^{2+}$ influx via tonically active Trp channels (Shoudai et al., 2010), release of $Ca^{2+}$ from intracellular stores (Llano et al., 2000), and resting cytosolic calcium (Kaeser and Regehr, 2014; Xu et al., 2009). Determining which sensors (e.g., syt1, Doc2α, Doc2β) decode $Ca^{2+}$-signaling from these various sources, and how these sources may differentially influence various neuronal populations, is an intriguing area for future study that may offer further insights into the mechanism and control of spontaneous neurotransmission.

## STAR Methods

### CONTACT FOR REAGENT AND RESOURCE SHARING

Further information and requests for resources and reagents should be directed to and will be fulfilled by Dr. Edwin Chapman (chapman@wisc.edu).

### EXPERIMENTAL MODEL AND SUBJECT DETAILS

All procedures involving animal models were performed in accordance with the guidelines of the National Institutes of Health and approved by the Animal Care and Use Committee at the University of Wisconsin - Madison. Most experiments were performed on hippocampal neurons cultured from postnatal mouse pups (P0-1) of various genetic strains, including: syt1-KO (Jackson Laboratory), Doc2α-KO, and Doc2β-KO mice (Groffen et al., 2010). All of these strains have the same genetic background (C57BL/6J). The sex of the pups used for these cultured neuron experiments was not determined. The RNAScope experiments were performed on cryosections obtained from healthy, male and female adult WT mice (4–7 weeks old) that were never involved with prior procedures. Mice were housed and cared for by the staff of the University of Wisconsin Research Animal Resources Center at the WIMR Vivarium facility. Cell lines used for this study (HEK293T/17 and PC12 cells) were cultured as described in the relevant Methods Details section, and were not tested for authentication.

### METHOD DETAILS

**Neuronal Cultures and Lentivirus—**Hippocampal neuronal cultures were prepared from syt1 (Jackson Laboratory), Doc2α,and Doc2β-KO mice (Groffen et al., 2010). Mice were maintained as heterozygous breeder pairs, and pups were used for cultures at postnatal day 0–1. All procedures were in accordance with the guidelines of the National Institutes of Health and approved by the Animal Care and Use Committee at the University of Wisconsin. For all recordings, WT littermates were used as controls. Briefly, hippocampi were dissected from mouse brain, digested for 20 min at 37° C in 0.25% trypsin-EDTA

(Gibco), mechanically dissociated, and plated at a density of ~100,000 cells/$cm^2$ onto 12 mm glass coverslips (Carolina Biological Supply) coated with poly-D-lysine. Cultures were grown in Neurobasal A medium (Gibco) supplemented with B27 (2%, Gibco) and GlutaMAX (2 mM, Gibco) and maintained at 37°C in a 5% $CO_2$ humidified incubator.

For experiments involving lentivirus, DNA sequences encoding full-length WT Doc2α, Doc2α mutants, WT Doc2β, Doc2β mutants, WT syt1, and syt1 mutants were subcloned into a FUGW transfer plasmid (Lois et al., 2002) modified with a synapsin promoter and an IRES-expressed soluble eGFP marker. Lentiviral particles were generated by co-transfection of the transfer plasmid and helper plasmids (pCD/NL-BH*ΔΔΔ and VSV-G encoded in pLTR-G) (Kutner et al., 2009) into HEK293T/17 cells. HEK293T/17 cells were grown in DMEM (Gibco) supplemented with 10% FBS (Atlanta Biological) and penicillin/streptomycin, passaged when they were ~90% confluent via trypsinization, and utilized only for their first 20 passages. Following transfection, the supernatant was collected after 48–72 hrs of expression, filtered through a 0.45 μm PVDF filter, and concentrated by ultra-centrifugation at 110,000×g for 2 hrs (Kutner et al., 2009). Viral particles were re-suspended in $Ca^{2+}$/$Mg^{2+}$-free PBS and used to infect neurons at day-in-vitro (DIV) 6. Successful infection and expression was monitored by live-cell imaging of the co-expressed GFP and by immunocytochemistry (please see below for detailed methods) comparing GFP expression (Abcam, rabbit, 1:1000) against a neuronal marker, MAP2 (Millipore, chicken, 1:1000). By this measure, greater than 95% of neurons were infected in all experiments.

For $Ca^{2+}$-imaging experiments, murine hippocampal neurons were cultured on 18 mm #1.5 coverslips and transfected at 5 DIV with a presynaptic fluorescent $Ca^{2+}$ indicator, syp-GCaMP6s, by calcium phosphate precipitation. Syp-GCaMP6s was generated by appending GCaMP6s to the C-terminus of synaptophysin using a 14-residue linker [$GS(GSS)_4$] linker and expressed under an EF1α promoter (Matsuda and Cepko, 2004).

**Electrophysiology—**Whole-cell voltage-clamp recordings were carried out using a Multiclamp 700B amplifier (Molecular Devices) at 16–19 DIV. Recordings were made at room temperature in a bath solution containing (in mM): 128 NaCl, 5 KCl, 1.2 $CaCl_2$, 1 $MgCl_2$, 30 D-glucose and 25 HEPES, pH 7.3 and 305 mOsm. Where indicated, $CaCl_2$ was increased to 2.4 or 10 mM. Patch pipettes (3 – 5 MΩ) were pulled from borosilicate glass (Sutter Instruments). When recording mEPSCs, the pipette internal solution contained (in mM): 130 K-Gluconate, 1 EGTA, 10 HEPES, 2 ATP, 0.3 GTP, and 5 sodium phosphocreatine, pH 7.35 and 275 mOsm. When recording mIPSCs, KCl was used instead of K-Gluconate at the same concentration. Data were acquired using a Digidata 1440A (Molecular Devices) and Clampex 10 software (Molecular Devices) at 10 kHz. Neurons were held at −70 mV. Series resistance was compensated and recordings were discarded if the access resistance rose above 15 MΩ at any point. Tetrodotoxin (TTX, 1 μM, Abcam) was included in the bath solution to isolate miniature events. When recording mEPSCs, AMPA-receptors were pharmacologically isolated with D-AP5 (50 μM, Abcam) and picrotoxin (100 μM, Abcam). When recording mIPSCs, $GABA_A$ receptors were pharmacologically isolated with D-AP5 (50 μM, Abcam) and CNQX (20 μM, Abcam). Recorded traces were analyzed using Clampfit 10 (Molecular Devices). Where applicable, pharmacological agents were

applied via bath perfusion (1–2 ml per minute flow rate, 0.75 ml total bath volume, typically applied for 5–20 minutes until a constant effect was observed).

**PC12 Cell Culture, Transfection, and Translocation Assays—**PC12 cells were cultured on 18 mm glass coverslips (Warner Instruments) coated with poly-D-lysine and collagen IV. Cells were grown in DMEM (Gibco) supplemented with 5% FBS (Atlanta Biological) and 5% horse serum (Atlanta Biological) and maintained at 37°C in a 10% $CO_2$ humidified incubator. One day before imaging experiments, each coverslip was transfected with 2.5 μg of DNA using Lipofectamine LTX (Invitrogen). For these experiments, DNA sequences encoding full-length WT and mutant forms of Doc2α and β were subcloned into a pEF vector (Matsuda and Cepko, 2004) and were tagged at the C-terminus with a flexible linker (GS-(GSS)x4) followed by eGFP. At 24 hrs following transfection, coverslips were transferred to an imaging chamber and bathed in an imaging solution containing (in mM): 145 NaCl, 2.8 KCl, 2 $CaCl_2$, 1 $MgCl_2$, 10 D-glucose and 10 HEPES, pH 7.3 and 305 mOsm. Cells were imaged using an Olympus FV1000 confocal microscope and a 20x/1.0 numerical aperture (NA) objective before and after stimulation by the addition of ionomycin (15 μM final concentration) to monitor the subcellular localization of the GFP-tagged protein. Line scan analysis was performed on individual cells before and after treatment with ionomycin using ImageJ 1.50b software (NIH). Plasma membranes (PM) were visually identified as the edge regions adjacent to the background intensity and the cytosol intensity was defined as average intensity of the region between the PM at opposite ends of each cell. For each cell analyzed, the location of the line scan was the same for the control and stimulated images.

**Live Cell Imagining of Doc2-HaloTag Fusion Proteins—**The HaloTag ligand, $JF_{646}$, was generously supplied by the Lavis Lab (HHMI, Janelia Research Campus). Neuronal cultures were incubated in 50nM $JF_{646}$ for 30 min to fluorescently label the Doc2-HaloTag fusion proteins. These cultures were then washed once and imaged in a solution of 140 mM NaCl, 5 mM KCl, 2 mM CaCl2, 2 mM $MgCl_2$, 10 mM HEPES, and 10 mM glucose (pH 7.4). Images of live hippocampal cultures were acquired at room temperature using an Olympus FV1000 laser scanning confocal microscope, with PMT-based detection and a 20×/1.0NA water objective lens. All images were acquired with Olympus Fluoview software using identical laser and gain settings. Figure images were colored and smoothed in ImageJ. For clarity, the brightness and contrast of the images in Figure 7C, D were adjusted and these same adjustments were applied to the corresponding images of control cultures in Supplemental Figure 4 and 5.

For image quantification, synaptic boutons were identified by the presence of synaptophysin-mRuby3. The synaptophysin channel was thresholded to puncta and regions of interest (ROIs) were identified in ImageJ (Particle Analysis, 5–15 pixel ROIs). For Doc2 or GFP channels, a mean-filtered image (3 pixel radius of filtering) was subtracted from the raw image to detect local enrichment of either protein. Puncta were then identified by thresholding. Synapses, i.e. the ROIs identified in the synaptophysin channel, were considered to be positive for either GFP or Doc2 if they had a greater than 21% overlap with GFP or Doc2 puncta.

**Presynaptic $Ca^{2+}$ measurements—**Images of live hippocampal cultures were acquired at room temperature using an Olympus IX81 inverted microscope with a 60X 1.45 NA oil-immersion objective. Illumination was provided by a 300W xenon arc lamp (Lambda DG-4, Sutter) attenuated with the DG-4's on-board neutral density filter function. Excitation and emission filtering were achieved with a standard GFP filter set (49002, Chroma) and images were acquired using a sCMOS camera (Orca FLASH 4.0 v2+, Hamamatsu) with 2x2 binning. Images were acquired using Micro-Manager 1.4 (Open Imaging) software (Edelstein et al., 2010). Image analysis was performed in ImageJ. For each measurement, a Z-stack (4 um, 0.4 um/slice) was acquired and collapsed by maximum projection.

At 13–14 DIV, coverslips expressing syp-GCaMP6s were placed in same bath solution used for electrophysiological experiments, transferred to an imaging chamber (Warner), and allowed to equilibrate at room temperature for 5–10 minutes. After acquiring a baseline measurement, the bath solution was exchanged for a similar bath containing 0 mM $Ca^{2+}$, 30 μM BAPTA-AM, and 30 μM CPA. Neurons were allowed to rest for 20 minutes before image acquisition under these conditions.

Single-wavelength $Ca^{2+}$ indicators require in-situ calibration to account for the total indicator present in a given measurement. After imaging in the 0 mM $Ca^{2+}$/BAPTA/CPA condition, the bath was exchanged for normal bath solution containing 4 mM $Ca^{2+}$ and 30 μM ionomcyin to saturate Syp-GCaMP6s. After 5 minutes, a final stack was acquired. For analysis, 5-pixel (1.0 μM) diameter round ROIs (30–90 per field of view) were selected and their intensities were measured using ImageJ. A dark region of the field of view was used for background subtraction. For each field of view, the value obtained after ionomycin treatment was used to obtain $F_{max}$ for use in the rearranged Hill equation (de Juan-Sanz et al., 2017):

$$[Ca]_{syp} = K_d \left( \frac{F_{syp}/F_{max} - 1/R_f}{1 - F_{syp}/F_{max}} \right)^{1/n}$$

where $K_d$ is the dissociation constant of the indicator, $F_{syp}$ is the average fluorescence across all ROI's in the field of view, $R_f$ is the dynamic range of the indicator, and $n$ is the Hill coefficient. For $K_d$, $R_f$, and $n$, we used published *in vitro* measurements (Chen et al., 2013), allowing for a modest (~15%) reduction in $R_f$ to account for increased background and the imperfect overlap of ROIs with Syp-GCaMP6s signals at boutons. The [Ca] at a synapse was calculated using this equation for the baseline condition and after incubation with 0 mM $Ca^{2+}$/BAPTA/CPA.

**Immunoblotting—**Cell lysates were prepared by dissolving single neuronal coverslips in boiling lysis buffer (100 mM Tris-Cl, 200 mM DTT, 4% w/v SDS, 0.2% w/v bromophenol blue, 20% v/v glycerol, pH 6.8). Samples were run on a 4–12% NuPAGE Bis-Tris gradient gel (Invitrogen) and transferred to a nitrocellulose membrane (GE) for blotting. Blots were probed with an anti-synaptotagmin 1 antibody (mouse, 1:500, 48.1) and an anti-VCP antibody (mouse monoclonal, 1:1000, Abcam). Blots were visualized with HrP-conjugated secondary antibodies (goat anti-mouse IgG, 1:5000, Biorad). VCP was used as a loading

control. Blots were imaged using an Amersham Imager 600 (GE) and brightness/contrast was adjusted for publication in ImageJ.

**Immunocytochemistry—**Dissociated hippocampal neurons, cultured from either WT, syt1 KO, Doc2α KO, or Doc2β KO pups, were fixed with 4% paraformaldehyde in PBS, at 37°C, for 15 minutes. Fixed neurons were washed two times with PBS and then permeabilized, at RT, for 10 min in PBS with 0.2% saponin and 50 mM $NH_4Cl$. The fixed and permeabilized cells were then incubated for 1 hr in blocking buffer 1 (10% goat serum and 0.04% saponin in PBS) and then incubated for 1 hr in primary antibody diluted in blocking buffer 2 (PBS with 1% goat serum and 0.04% saponin). The mouse anti-VGAT antibody (SYnaptic SYstems) and the guinea pig anti-VGLUT antibody (Millipore) were diluted 1:500 and the chicken anti-MAP2 (Millipore) antibody was diluted 1:1000. Neurons were then washed four times in wash buffer (PBS with 0.04% saponin) and incubated for 1 hr in secondary antibody diluted in blocking buffer 2. The Alexa Fluor® 488 goat anti-mouse antibody and the Alexa Fluor® 568 goat anti-guinea pig antibody (Thermo Fischer Scientific) were diluted 1:400 and the Alexa Fluor® 647 goat anti-chicken antibody (Thermo Fischer Scientific) was diluted 1:800 in blocking buffer 2. After the secondary antibody incubation, neurons were washed once in wash buffer and three times in PBS before being mounted on glass slides in ProLong® Gold Antifade Mountant (Thermo Fischer Scientific). Images were acquired on an Olympus FV1000 laser scanning confocal microscope, with a 60x 1.4 NA oil immersion objective and PMT-based detection, using identical laser and gain settings for all samples. Images were adjusted in brightness and contrast. 10x4 micron regions of interest (7 – 11 per field of view) were analyzed and these regions of interest were centered on a non-overlapping dendrite marked by MAP2.

**RNA in situ hybridization—**Adult WT mice, 4–7 weeks old, were initially fixed via transcardial perfusion of PBS and then 4% paraformaldehyde (15 ml). Brains were dissected and post-fixed in 4% paraformaldehyde overnight (12–16hrs) at 4 degrees C. Brains were then sequentially equilibrated to 10% sucrose, 20% sucrose, and 30% sucrose before being flash-frozen in Optimal Cutting Temperature embedding media (Tissue-Tek). Coronal brain sections (10 μm) were cut using a cryostat (Leica) and mounted onto SuperFrost Plus slides (Fisher). Sections were stored at −80 degrees C prior to use. Next, brain sections were baked at 60 degrees C for 1 hr, fixed at room temperature in 4% paraformaldehyde for 1hr, and dehydrated at room temperature in 50% ethanol (5 min), 70% ethanol (5 min), and twice in 100% ethanol (5 min each). Slides were air dried at room temperature for 5 min.

RNA *in situ* hybridization (ISH) was performed using RNAscope Multiplex Fluorescent Reagent Kit v2 (Advanced Cell Diagnostics), following the manual step-wise. Probes used were catalogue probes Mm-Doc2β targeting 829 – 2440 of NM_007873.3 and Mm-Slc32a1 (VGAT) targeting 894–2037 of NM_009508.2, and a custom probe generated against Doc2α (Advanced Cell Diagnostics ID: Mm-Doc2α) targeting 845–2077 of NM_010069.1. Positive control probes (C1-POLR2A, C2-PPIB, C3-UBC, C4-HPRT) and negative control probes (targeting dapB, a bacterial gene) were provided alongside the RNAscope kit. Signal was visualized by conjugating the probes to the following fluorescent dyes (Opal Dyes Reagent Packs, PerkinElmer, 1:1,500 during the labeling reaction): Opal 520 (VGAT), Opal 570

(Doc2β), and Opal 620 (Doc2α). Sections were incubated in DAPI for 30 seconds before being sealed in ProLong Gold Antifade Mountant (Fisher Scientific).

The stained cryosections were imaged using a Lecia SP8 laser scanning confocal microscope equipped with a white light laser, HyD detectors, and a 63x/1.4NA oil objective. The excitation/emission profiles used for opal dyes 520, 570, and 620 were 494/499–544, 550/566–594, and 588/599–637, respectively. Images were acquired in sequence. Identical laser and gain settings for each channel, corresponding to a single opal dye, were used for all of the micrographs collected at high-magnification (63x) in this study. RNA staining signals were identified as punctate dots, with each dot corresponding to a single RNA transcript.

**Liposome preparation—**Liposomes were prepared from POPC, DOPS, POPE, and brain $PIP_2$ (Avanti Polar Lipids) stored individually as chloroform stocks, except for brain $PIP_2$ (stored in 20:9:1 $CHCl_3$:MeOH:$H_2O$). The lipids were combined, the solvent was evaporated under a stream of nitrogen, and the films were dried under vacuum for at least 2 hrs. Films were rehydrated in reconstitution buffer (100 mM KCl, 25 mM HEPES pH 7.4) at a final concentration of 10 mM [lipid] and extruded at least 30 times through a single 100-nm polycarbonate filter (Whatman), yielding liposomes of ~100 nm in diameter. Lipid compositions included 25% DOPS, 30% POPE, and 45% POPC, with POPC replacing DOPS in the 0% DOPS formulations and $PIP_2$ replacing POPC in the 1–3% $PIP_2$ formulations.

**Protein purification—**Constructs encoding Syt1 C2AB (a.a. 96–421) and Doc2β C2AB (a.a. 125–407) were expressed as GST fusion proteins (pGEX-4T vector, GE) in *E. Coli*, purified via glutathione-Sepharose affinity chromatography, and cleaved with thrombin in 100 mM KCl, 25 mM HEPES pH 7.4, 5% glycerol. Halo-C2AB constructs were assembled by overlap extension PCR and subcloned into pTrcHis A vector (ThermoFisher) to yield N-terminal $His_6$-HaloTag-C2AB constructs. These constructs were expressed in *E. Coli*, purified via Nickel-NTA chromatography, and eluted in His-tag elution buffer (500 mM imidazole, 400 mM KCl, 25 mM HEPES pH 7.4, and 10% glycerol). The SNAP-25B-syntaxin1a heterodimer was subcloned into the pRSF Duet vector (Novagen) with the $His_6$-tag on the N-terminus of SNAP-25, expressed in *E. Coli*, purified via nickel-NTA chromatography, and eluted in His-tag elution buffer containing 1% octylglucoside and 2 mM DTT.

**Equilibrium cosedimentation assays—**Liposomes (2 mM), C2AB (4 μM), and EGTA (0.2 mM) were combined and brought up to 100 μl in reconstitution buffer with or without 0.7 mM $CaCl_2$ added. The mixture was incubated for 15 min at room temperature with shaking, loaded into a polycarbonate centrifuge tube, and centrifuged at 65,000 RPM for 30 min in a TLA-100 rotor (Beckman). An aliquot of the supernatant was combined 1:1 with 2x SDS sample buffer and subjected to SDS-PAGE. Gels were stained with Coomassie blue, imaged, and the bands quantified using ImageJ. $Ca^{2+}$ titrations were performed similarly, with the substitution of BAPTA (3 mM) for EGTA. $CaCl_2$ additions to achieve the desired free [$Ca^{2+}$] were calculated using the WebMaxC Standard application (https://web.stanford.edu/~cpatton/webmaxcS.htm).

**HaloTag SNARE-binding assays—**Purified $His_6$-Halo-C2AB constructs (100 μg) were combined with HaloLink resin (100 μL bed volume), and the mixture was brought up to 500 μL with binding buffer (150 mM KCl, 25 mM HEPES pH 7.4, 1% Triton X-100) and incubated 30 min at room temperature with rotation. Complete depletion of Halo-C2AB from the supernatant under these conditions was verified by SDS-PAGE. Halo-C2AB-bearing beads were washed 3x in binding buffer and resuspended as a 50% slurry. Forty μL of this slurry was added to a 150 μL binding reaction containing 2.5 μM t-SNAREs, 1 mM EGTA ± 1.5 mM $Ca^{2+}$, and 1 mM DTT in binding buffer, and the mixture was incubated for 1 hr at room temperature. The beads were then washed 3x in binding buffer containing 1 mM EGTA ± 1.5 mM $Ca^{2+}$, and the t-SNAREs were eluted in 35 μL 2x SDS sample buffer. For each sample, 15 μL of the eluate was subject to SDS-PAGE, the gels were imaged after staining with Coomassie Blue, and the band intensities quantified in ImageJ with background subtraction and normalization to a heterodimer loading control in each gel. For each gel, 2 μg of each $His_6$-HaloTag-C2AB fusion construct and 2.5 μg of t-SNARE heterodimer were loaded as standards, and $His_6$-HaloTag expressed without a fusion partner was used as a negative control.

**Materials and Reagents—**TTX, D-AP5, CNQX, picrotoxin, BAPTA-AM, and cyclopiazonic acid (CPA) were obtained from Abcam. Purified lipids used in biochemical assays were obtained from Avanti Polar Lipids. Cell culture reagents were supplied by Gibco and Atlanta Biological. Unless otherwise noted, other chemical reagents were obtained from Sigma.

## QUANTIFICATION AND STATISTICAL ANALYSIS

Values are reported, in both the text and figures, as mean ± standard error of the mean (SEM). For electrophysiological experiments, each “n” represents the measurement from a single cell or neuron and “n’s” were obtained from at least three individual animal preparations. Other experimental designs indicate the definition of an “n” in the accompanying Results text or Figure Legend. Graphically, bars represent the mean value and error bars denoted the standard error. Unless otherwise noted, statistical analysis was conducted using a Student’s t-test when data was normally distributed. In the case of multiple comparisons, ANOVA tests were conducted and data were further analyzed with the appropriate post-hoc test for the indicated individual comparisons (i.e., Tukey’s test, Sidak’s test, and Dunnett’s multiple comparison test). For non-normally distributed datasets (assessed by D’Agostino-Pearson omnibus normality test), the nonparametric Mann-Whitney test (single comparison) or Kruskal-Wallis test (multiple comparisons) were used as appropriate. Expected sample sizes were not estimated or predetermined. All statistical analysis was conducted using GraphPad Prism 7.01 (GraphPad Software Inc).

## DATA AND SOFTWARE AVAILABILITY

Data available by request. No custom software or scripts were used in the course of this study.

## Supplementary Material

Refer to Web version on PubMed Central for supplementary material.

## Acknowledgments

We would like to acknowledge Luke Lavis (HHMI, Janelia Research Campus) for generously providing the JF646 Halo ligand, the WIMR Optical Imaging Core (University of Wisconsin - Madison) for their expertise and the use of their imaging equipment for the RNAScope experiments, and members of the Chapman lab for critical comments regarding this manuscript. This study was supported by grants from the US National Institutes of Health (MH061876 and R35NS097362 to E.R.C.). E.R.C. is an Investigator of the Howard Hughes Medical Institute.

## References

Bai H, Xue R, Bao H, Zhang L, Yethiraj A, Cui Q, Chapman ER. Different states of synaptotagmin regulate evoked versus spontaneous release. Nat. Commun. 2016; 7:10971. [PubMed: 27001899]

Bhalla A, Chicka MC, Tucker WC, Chapman ER. Ca2+–synaptotagmin directly regulates t-SNARE function during reconstituted membrane fusion. Nat. Struct. Mol. Biol. 2006; 13:323–330. [PubMed: 16565726]

Broadie K, Bellen HJ, DiAntonio A, Littleton JT, Schwarz TL. Absence of synaptotagmin disrupts excitation-secretion coupling during synaptic transmission. Proc. Natl. Acad. Sci. U. S. A. 1994; 91:10727–10731. [PubMed: 7938019]

Brose N, Petrenko AG, Sudhof TC, Jahn R. Synaptotagmin: a calcium sensor on the synaptic vesicle surface. Science. 1992; 256:1021–1025. [PubMed: 1589771]

Bucurenciu I, Bischofberger J, Jonas P. A small number of open Ca2+ channels trigger transmitter release at a central GABAergic synapse. Nat. Neurosci. 2010; 13:19–21. [PubMed: 20010820]

Carter AG, Regehr WG. Quantal events shape cerebellar interneuron firing. Nat. Neurosci. 2002; 5:1309–1318. [PubMed: 12411959]

Chapman ER. How Does Synaptotagmin Trigger Neurotransmitter Release? Annu. Rev. Biochem. 2008; 77:615–641. [PubMed: 18275379]

Chen T-W, Wardill TJ, Sun Y, Pulver SR, Renninger SL, Baohan A, Schreiter ER, Kerr RA, Orger MB, Jayaraman V, et al. Ultra-sensitive fluorescent proteins for imaging neuronal activity. Nature. 2013; 499:295–300. [PubMed: 23868258]

Chicka MC, Hui E, Liu H, Chapman ER. Synaptotagmin arrests the SNARE complex before triggering fast, efficient membrane fusion in response to Ca2+ Nat. Struct. Mol. Biol. 2008; 15:827–835. [PubMed: 18622390]

Edelstein A, Amodaj N, Hoover K, Vale R, Stuurman N. Computer Control of Microscopes Using μManager. Curr. Protoc. Mol. Biol. 2010; 92:14.20.1–14.20.17.

Ehlers MD, Heine M, Groc L, Lee MC, Choquet D. Diffusional Trapping of GluR1 AMPA Receptors by Input-Specific Synaptic Activity. Neuron. 2007; 54:447–460. [PubMed: 17481397]

Farrant M, Nusser Z. Variations on an inhibitory theme: phasic and tonic activation of GABAA receptors. Nat. Rev. Neurosci. 2005; 6:215–229. [PubMed: 15738957]

Frank CA, Kennedy MJ, Goold CP, Marek KW, Davis GW. Mechanisms Underlying the Rapid Induction and Sustained Expression of Synaptic Homeostasis. Neuron. 2006; 52:663–677. [PubMed: 17114050]

Friedrich R, Groffen AJ, Connell E, van Weering JRT, Gutman O, Henis YI, Davletov B, Ashery U. DOC2B Acts as a Calcium Switch and Enhances Vesicle Fusion. J. Neurosci. 2008; 28:6794–6806. [PubMed: 18596155]

Friedrich R, Yeheskel A, Ashery U. DOC2B, C2 Domains, and Calcium: A Tale of Intricate Interactions. Mol. Neurobiol. 2010; 41:42–51. [PubMed: 20052564]

Gaffaney JD, Xue R, Chapman ER. Mutations that disrupt Ca2+-binding activity endow Doc2β with novel functional properties during synaptic transmission. Mol. Biol. Cell. 2014; 25:481–494. [PubMed: 24356452]

Giladi M, Michaeli L, Almagor L, Bar-On D, Buki T, Ashery U, Khananshvili D, Hirsch JA. The C2B Domain Is the Primary Ca2 + Sensor in DOC2B: A Structural and Functional Analysis. J. Mol. Biol. 2013; 425:4629–4641. [PubMed: 23994332]

Groffen AJ, Martens S, Arazola RD, Cornelisse LN, Lozovaya N, de Jong APH, Goriounova NA, Habets RLP, Takai Y, Borst JG, et al. Doc2b is a High Affinity Ca2+ Sensor for Spontaneous Neurotransmitter Release. Science. 2010; 327:1614–1618. [PubMed: 20150444]

Groffen AJA, Brian EC, Dudok JJ, Kampmeijer J, Toonen RF, Verhage M. Ca2+-induced Recruitment of the Secretory Vesicle Protein DOC2B to the Target Membrane. J. Biol. Chem. 2004; 279:23740–23747. [PubMed: 15033971]

Groffen AJA, Friedrich R, Brian EC, Ashery U, Verhage M. DOC2A and DOC2B are sensors for neuronal activity with unique calcium-dependent and kinetic properties. J. Neurochem. 2006; 97:818–833. [PubMed: 16515538]

Guan Z, Bykhovskaia M, Jorquera RA, Sutton RB, Akbergenova Y, Littleton JT. A synaptotagmin suppressor screen indicates SNARE binding controls the timing and Ca2+ cooperativity of vesicle fusion. ELife. 2017; 6:e28409. [PubMed: 28895532]

Jones HC, Keep RF. Brain fluid calcium concentration and response to acute hypercalcaemia during development in the rat. J. Physiol. 1988; 402:579–593. [PubMed: 3236250]

de Juan-Sanz J, Holt GT, Schreiter ER, de Juan F, Kim DS, Ryan TA. Axonal Endoplasmic Reticulum Ca2+ Content Controls Release Probability in CNS Nerve Terminals. Neuron. 2017; 93:867–881.e6. [PubMed: 28162809]

Kaeser PS, Regehr WG. Molecular Mechanisms for Synchronous, Asynchronous, and Spontaneous Neurotransmitter Release. Annu. Rev. Physiol. 2014; 76:333–363. [PubMed: 24274737]

Kojima T, Fukuda M, Aruga J, Mikoshiba K. Calcium-Dependent Phospholipid Binding to the C2A Domain of a Ubiquitous Form of Double C2 Protein (Doc2β). J. Biochem. (Tokyo). 1996; 120:671–676. [PubMed: 8902635]

Kombian SB, Hirasawa M, Mouginot D, Chen X, Pittman QJ. Short-Term Potentiation of Miniature Excitatory Synaptic Currents Causes Excitation of Supraoptic Neurons. J. Neurophysiol. 2000; 83:2542–2553. [PubMed: 10805656]

Kutner RH, Zhang X-Y, Reiser J. Production, concentration and titration of pseudotyped HIV-1-based lentiviral vectors. Nat. Protoc. 2009; 4:495–505. [PubMed: 19300443]

Liu H, Dean C, Arthur CP, Dong M, Chapman ER. Autapses and networks of hippocampal neurons exhibit distinct synaptic transmission phenotypes in the absence of synaptotagmin I. J. Neurosci. 2009; 29:7395–7403. [PubMed: 19515907]

Liu H, Bai H, Xue R, Takahashi H, Edwardson JM, Chapman ER. Linker mutations dissociate the function of synaptotagmin I during evoked and spontaneous release and reveal membrane penetration as a step during excitation-secretion coupling. Nat. Neurosci. 2014; 17:670–677. [PubMed: 24657966]

Llano I, González J, Caputo C, Lai FA, Blayney LM, Tan YP, Marty A. Presynaptic calcium stores underlie large-amplitude miniature IPSCs and spontaneous calcium transients. Nat. Neurosci. 2000; 3:1256–1265. [PubMed: 11100146]

Lois C, Hong EJ, Pease S, Brown EJ, Baltimore D. Germline Transmission and Tissue-Specific Expression of Transgenes Delivered by Lentiviral Vectors. Science. 2002; 295:868–872. [PubMed: 11786607]

Matsuda T, Cepko CL. Electroporation and RNA interference in the rodent retina in vivo and in vitro. Proc. Natl. Acad. Sci. U. S. A. 2004; 101:16–22. [PubMed: 14603031]

McKinney RA, Capogna M, Dürr R, Gähwiler BH, Thompson SM. Miniature synaptic events maintain dendritic spines via AMPA receptor activation. Nat. Neurosci. 1999; 2:44–49. [PubMed: 10195179]

Nishiki T, Augustine GJ. Dual Roles of the C2B Domain of Synaptotagmin I in Synchronizing Ca2+-Dependent Neurotransmitter Release. J. Neurosci. 2004; 24:8542–8550. [PubMed: 15456828]

Pang ZP, Bacaj T, Yang X, Zhou P, Xu W, Südhof TC. Doc2 supports spontaneous synaptic transmission by a Ca2+-independent mechanism. Neuron. 2011; 70:244–251. [PubMed: 21521611]

Ramirez DM, Kavalali ET. Differential regulation of spontaneous and evoked neurotransmitter release at central synapses. Curr. Opin. Neurobiol. 2011; 21:275–282. [PubMed: 21334193]

Reese AL, Kavalali ET. Single synapse evaluation of the postsynaptic NMDA receptors targeted by evoked and spontaneous neurotransmission. ELife. 2016; 5:e21170. [PubMed: 27882871]

Shahrezaei V, Cao A, Delaney KR. Ca2+ from One or Two Channels Controls Fusion of a Single Vesicle at the Frog Neuromuscular Junction. J. Neurosci. 2006; 26:13240–13249. [PubMed: 17182774]

Shoudai K, Peters JH, McDougall SJ, Fawley JA, Andresen MC. Thermally active TRPV1 tonically drives central spontaneous glutamate release. J. Neurosci. 2010; 30:14470–14475. [PubMed: 20980604]

Stanley EF. Single calcium channels and acetylcholine release at a presynaptic nerve terminal. Neuron. 1993; 11:1007–1011. [PubMed: 8274272]

Sutton MA, Schuman EM. Dendritic protein synthesis, synaptic plasticity, and memory. Cell. 2006; 127:49–58. [PubMed: 17018276]

Sutton MA, Wall NR, Aakalu GN, Schuman EM. Regulation of Dendritic Protein Synthesis by Miniature Synaptic Events. Science. 2004; 304:1979–1983. [PubMed: 15218151]

Sutton MA, Ito HT, Cressy P, Kempf C, Woo JC, Schuman EM. Miniature Neurotransmission Stabilizes Synaptic Function via Tonic Suppression of Local Dendritic Protein Synthesis. Cell. 2006; 125:785–799. [PubMed: 16713568]

Tsintsadze T, Williams CL, Weingarten DJ, Gersdorff H von, Smith SM. Distinct Actions of Voltage-Activated Ca2+ Channel Block on Spontaneous Release at Excitatory and Inhibitory Central Synapses. J. Neurosci. 2017; 37:4301–4310. [PubMed: 28320843]

Tucker WC, Weber T, Chapman ER. Reconstitution of Ca2+-Regulated Membrane Fusion by Synaptotagmin and SNAREs. Science. 2004; 304:435–438. [PubMed: 15044754]

Verderio C, Pozzi D, Pravettoni E, Inverardi F, Schenk U, Coco S, Proux-Gillardeaux V, Galli T, Rossetto O, Frassoni C, et al. SNAP-25 Modulation of Calcium Dynamics Underlies Differences in GABAergic and Glutamatergic Responsiveness to Depolarization. Neuron. 2004; 41:599–610. [PubMed: 14980208]

Verhage M, de Vries KJ, Røshol H, Burbach JPH, Gispen WH, Südhof TC. DOC2 Proteins in Rat Brain: Complementary Distribution and Proposed Function as Vesicular Adapter Proteins in Early Stages of Secretion. Neuron. 1997; 18:453–461. [PubMed: 9115738]

Vyleta NP, Smith SM. Spontaneous glutamate release is independent of calcium influx and tonically activated by the calcium-sensing receptor. J. Neurosci. 2011; 31:4593–4606. [PubMed: 21430159]

Wierda KDB, Sørensen JB. Innervation by a GABAergic Neuron Depresses Spontaneous Release in Glutamatergic Neurons and Unveils the Clamping Phenotype of Synaptotagmin-1. J. Neurosci. 2014; 34:2100–2110. [PubMed: 24501351]

Williams C, Chen W, Lee C-H, Yaeger D, Vyleta NP, Smith SM. Coactivation of multiple tightly-coupled calcium channels triggers spontaneous release of GABA. Nat. Neurosci. 2012; 15:1195–1197. [PubMed: 22842148]

Xu J, Pang ZP, Shin O-H, Südhof TC. Synaptotagmin-1 functions as the Ca2+-sensor for spontaneous release. Nat. Neurosci. 2009; 12:759–766. [PubMed: 19412166]

Xue R, Gaffaney JD, Chapman ER. Structural elements that underlie Doc2β function during asynchronous synaptic transmission. Proc. Natl. Acad. Sci. U. S. A. 2015; 112:E4316–E4325. [PubMed: 26195798]

Yao J, Gaffaney JD, Kwon SE, Chapman ER. Doc2 is a Ca2+ sensor required for asynchronous neurotransmitter release. Cell. 2011; 147:666–677. [PubMed: 22036572]

Zhang S, Xu M, Miao Q, Poo M, Zhang X. Endocannabinoid-Dependent Homeostatic Regulation of Inhibitory Synapses by Miniature Excitatory Synaptic Activities. J. Neurosci. 2009; 29:13222–13231. [PubMed: 19846710]

Zhou Q, Lai Y, Bacaj T, Zhao M, Lyubimov AY, Uervirojnangkoorn M, Zeldin OB, Brewster AS, Sauter NK, Cohen AE, et al. Architecture of the Synaptotagmin-SNARE Machinery for Neuronal Exocytosis. Nature. 2015; 525:62–67. [PubMed: 26280336]

Zhou Q, Zhou P, Wang AL, Wu D, Zhao M, Südhof TC, Brunger AT. The primed SNARE–complexin–synaptotagmin complex for neuronal exocytosis. Nature. 2017; 548:420–425. [PubMed: 28813412]

## Highlights

1. Synaptotagmin-1, Doc2α and Doc2β are $Ca^{2+}$ sensors that drive spontaneous release.
2. Doc2α is expressed in glutamatergic neurons and solely promotes mEPSCs.
3. Doc2β is expressed in GABAergic neurons and promotes mIPSCs along with syt1.
4. Syt1, but not Doc2α/β, senses $Ca^{2+}$ entry via VGCCs when promoting minis.

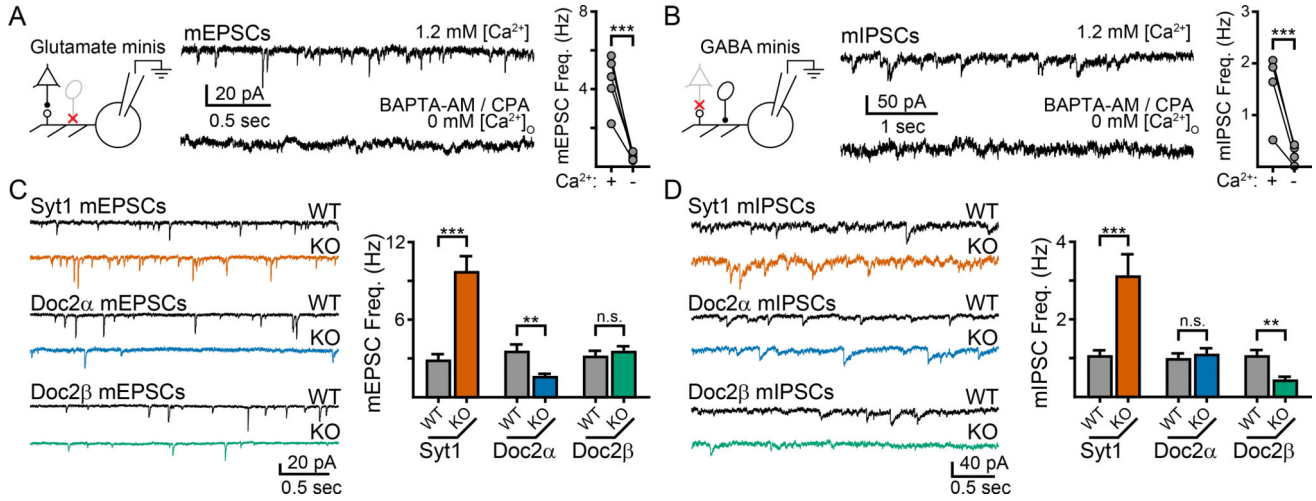


**Figure 1.**

Single KO of syt1, Doc2α, and Doc2β results in different phenotypes for spontaneous excitatory and inhibitory neurotransmission in cultured mouse hippocampal neurons. **A.** (Left) Schematic of the recording paradigm illustrating that glutamatergic transmission was isolated by inhibiting $GABA_A$-receptors. Glutamatergic neuron: triangle, GABAergic neuron: oval. Representative traces (center) and quantification (right) demonstrating that most AMPA-receptor mediated mEPSCs require the presence of $Ca^{2+}$. **B.** Schematic (left), representative traces (center), and quantification (right) demonstrating that $GABA_A$-receptor mediated mIPSCs are also strongly dependent on $Ca^{2+}$. **C.** Representative traces (left) and quantification (right) of the effect of single KO of syt1 (orange), Doc2α (blue), and Doc2β (green) on mEPSC frequency compared to WT littermate controls. Syt1 KO resulted in an 'unclamped' phenotype and an increase in mEPSC frequency, while Doc2α KO significantly reduced mEPSC frequency. Loss of Doc2β had no effect. **D.** Same as panel (c), but examining mIPSCs. Syt1 KO again resulted in an 'unclamped' phenotype whereas Doc2β KO significantly reduced mIPSC frequency; loss of Doc2α had no effect. ** denotes $p < 0.01$, *** denotes $p < 0.001$, n.s. denotes $p > 0.05$. Bar graphs represent mean ± SEM. See also Supp. Fig. 1 and 2.

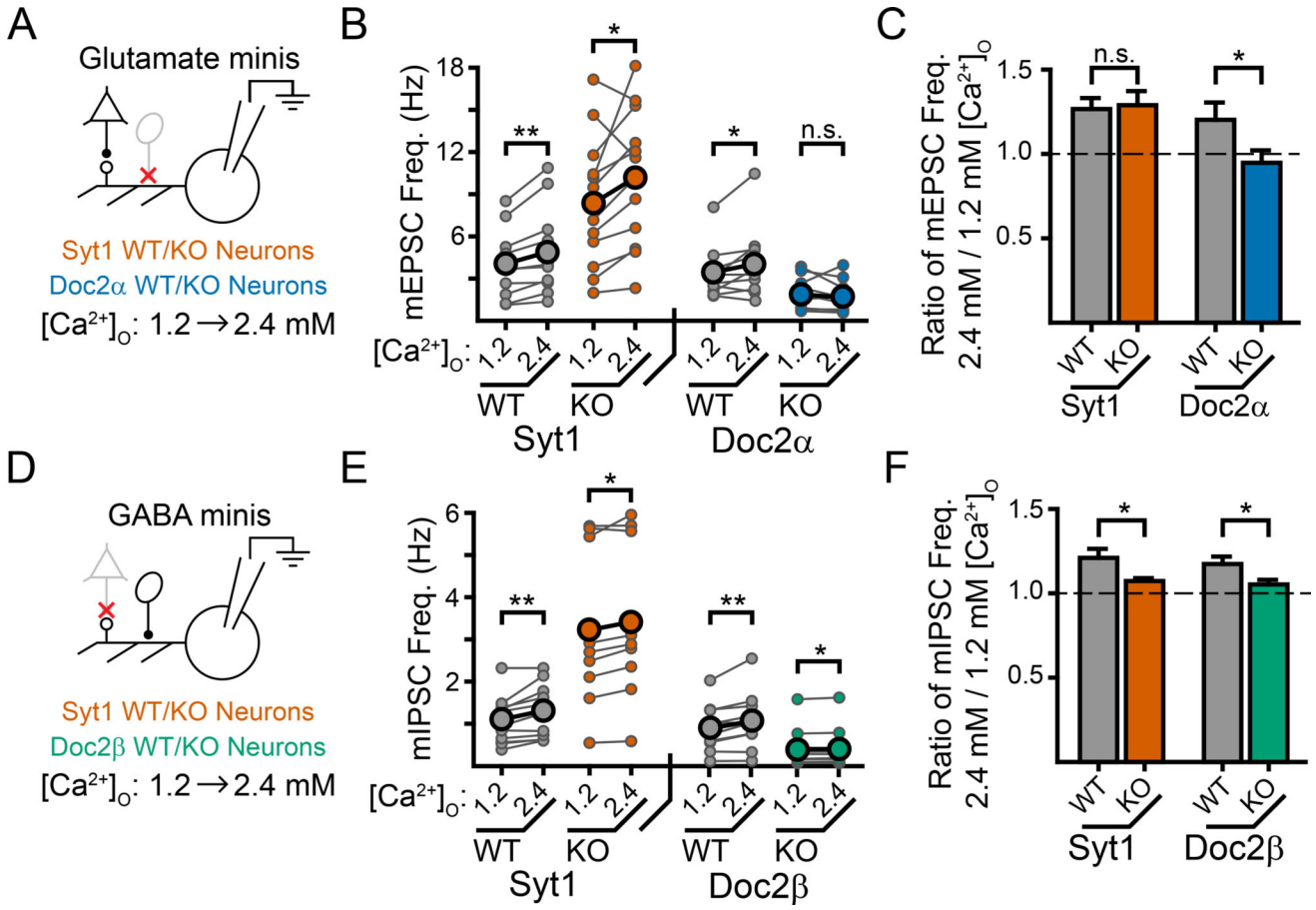


**Figure 2.**

Doc2α, but not syt1, promotes $Ca^{2+}$-dependent mEPSCs in a physiological range of $[Ca^{2+}]_O$ while both Doc2β and syt1 promote $Ca^{2+}$-dependent mIPSCs. **A.** Cartoon schematic of the experimental paradigm. Recordings were made first in 1.2 mM $[Ca^{2+}]_O$ before changing the bath solution to 2.4 mM $[Ca^{2+}]_O$. mEPSCs were then recorded again, from the same cell, in 2.4 mM $[Ca^{2+}]_O$. **B.** Quantification of mEPSC frequency for each recording denoted as a connected pair of smaller circles. The larger circles indicate the average values. **C.** Quantification of the normalized increase in mEPSC frequency induced by higher $[Ca^{2+}]_O$. Loss of Doc2α abolished this $Ca^{2+}$-dependent increase while loss of syt1 had no effect. **D–F)** Experiments were carried out exactly as described in Fig. 2, but examined mIPSCs rather than mEPSCs. Loss of either Doc2β or syt1 reduced, but did not abolish, this $Ca^{2+}$-dependent increase in mini frequency observed when bath $[Ca^{2+}]_O$ was increased from 1.2 to 2.4 mM. * denotes $p < 0.05$, ** denotes $p < 0.01$, *** denotes $p < 0.001$, n.s. denotes $p > 0.05$. Bar graphs represent mean ± SEM. See also Supp. Fig. 3.

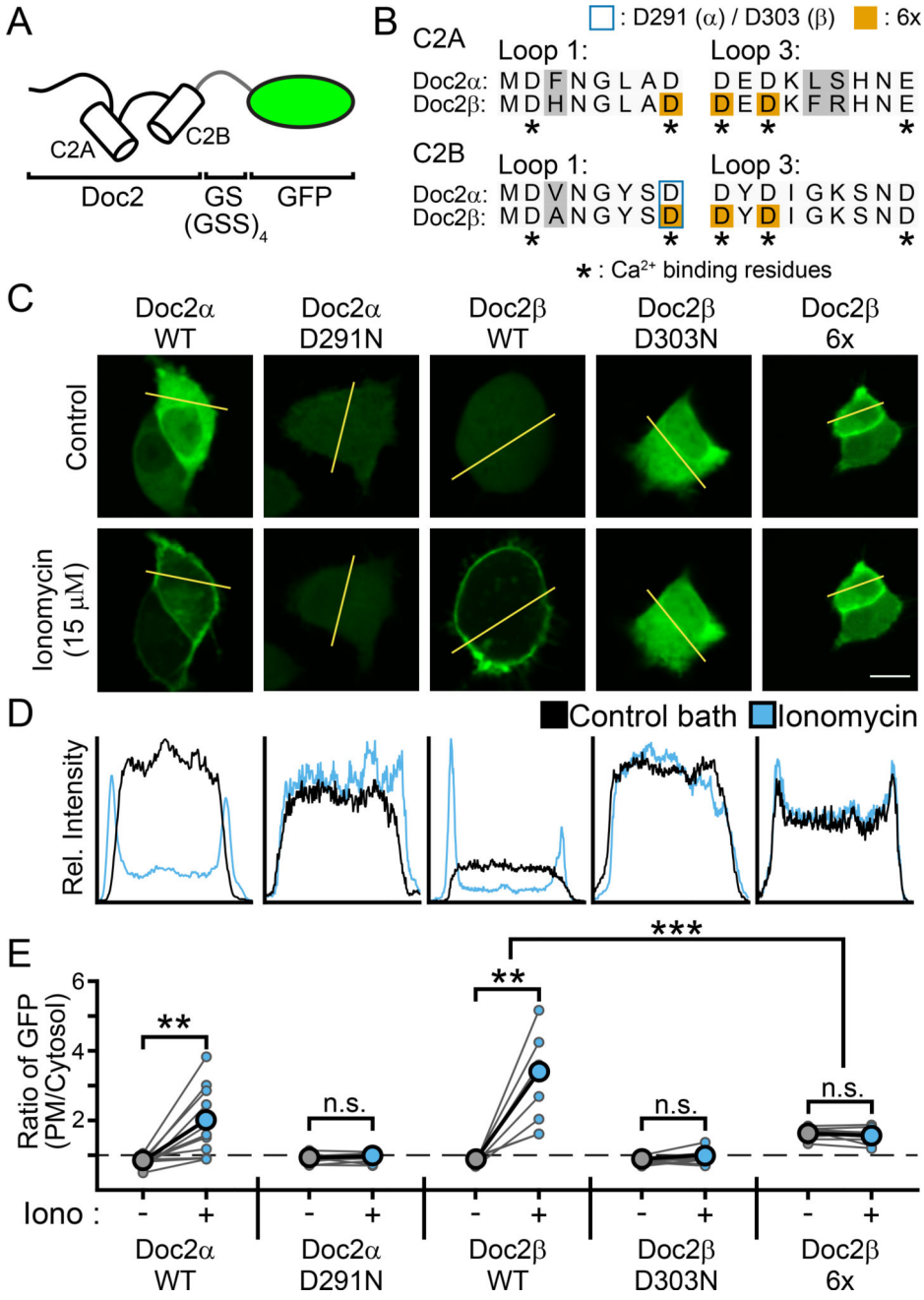


**Figure 3.**

Translocation assays demonstrating that mutations in Doc2 can result in either loss-or gain-of-function. **A.** Doc2α and β were tagged at their C-termini with GFP for visualization of their subcellular distribution when expressed in PC12 cells. **B.** Sequence alignment of the $Ca^{2+}$-binding loops of Doc2α and β. In C2A, loop 1 corresponds to aa 122–129 / 156–163 (α / β) and loop 3 corresponds to AA 184–192 / 218–226 (Friedrich et al., 2010). In C2B, loops 1 and 3 correspond to residues 284–291 / 296–303 and 345–353 / 357–365, respectively (Giladi et al., 2013). The loops of Doc2α were determined by sequence alignment with Doc2β. Grey backgrounds highlight differences between the isoforms.

Asterisks denote residues that serve as $Ca^{2+}$ ligands. Substituted residues are denoted by either a blue border (Doc2α D291, Doc2β D303) or an orange background (Doc2β 6x). **C.** Representative PC12 cells that were transfected with GFP-tagged WT or mutant Doc2α or β in control conditions (top) or when treated with ionomycin (bottom). Scale bar represents 10 μm. **D.** Line-scans of the cells in *panel (C)* (denoted by the yellow line) quantifying the subcellular distribution of Doc2 (as measured by GFP intensity). A single, representative line scan was performed for each cell analyzed. **E.** Quantification of the ratio of GFP intensity at the PM divided by the average intensity in the cytosol for each PC12 cell imaged. Connected dots represent the same cell before and after addition of ionomycin. * denotes $p < 0.05$, ** denotes $p < 0.01$, *** denotes $p < 0.001$, n.s. denotes $p > 0.05$.

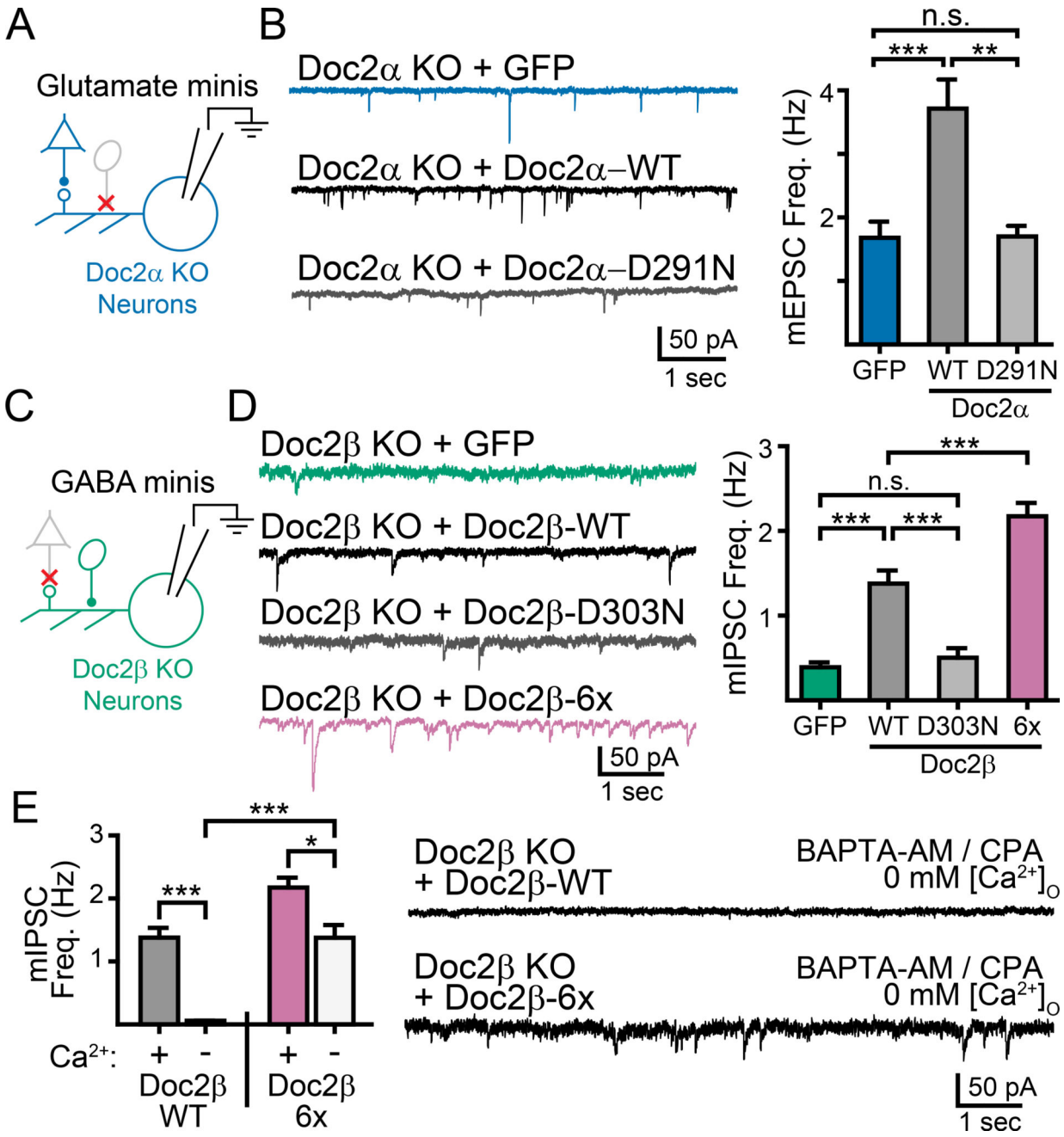


**Figure 4.**

Doc2α and β are direct $Ca^{2+}$-sensors driving spontaneous glutamate and GABA release. **A.** The indicated Doc2α constructs were expressed in Doc2α KO neurons using lentivirus. **B.** Representative traces (left) and quantification (right) of recordings in Doc2α KO neurons expressing a control (GFP), Doc2α WT, or Doc2α D291N. An ANOVA test comparing the rates for all constructs was significant with $p < 0.001$, graphical comparisons represent pairwise post-hoc tests. **C.** Doc2β constructs were expressed in Doc2β KO neurons using lentivirus. **D.** Representative traces (left) and quantification (right) of recordings in Doc2β KO neurons expressing a control (GFP), Doc2β-WT, or a mutant construct of Doc2β. An

ANOVA test comparing the rates for all constructs was significant with $p < 0.001$, graphical comparisons represent pairwise post-hoc tests. **E.** Quantification (left) and traces (right) of mIPSC recordings made in the absence of $Ca^{2+}$ in Doc2β KO neurons rescued with either Doc2β WT or Doc2β 6x. Remarkably, expression of Doc2β 6x mutant allowed significant miniature release to occur in the absence of $Ca^{2+}$. * denotes $p < 0.05$, ** denotes $p < 0.01$, *** denotes $p < 0.001$, n.s. denotes $p > 0.05$. Bar graphs represent mean ± SEM. See also Supp. Fig. 4.

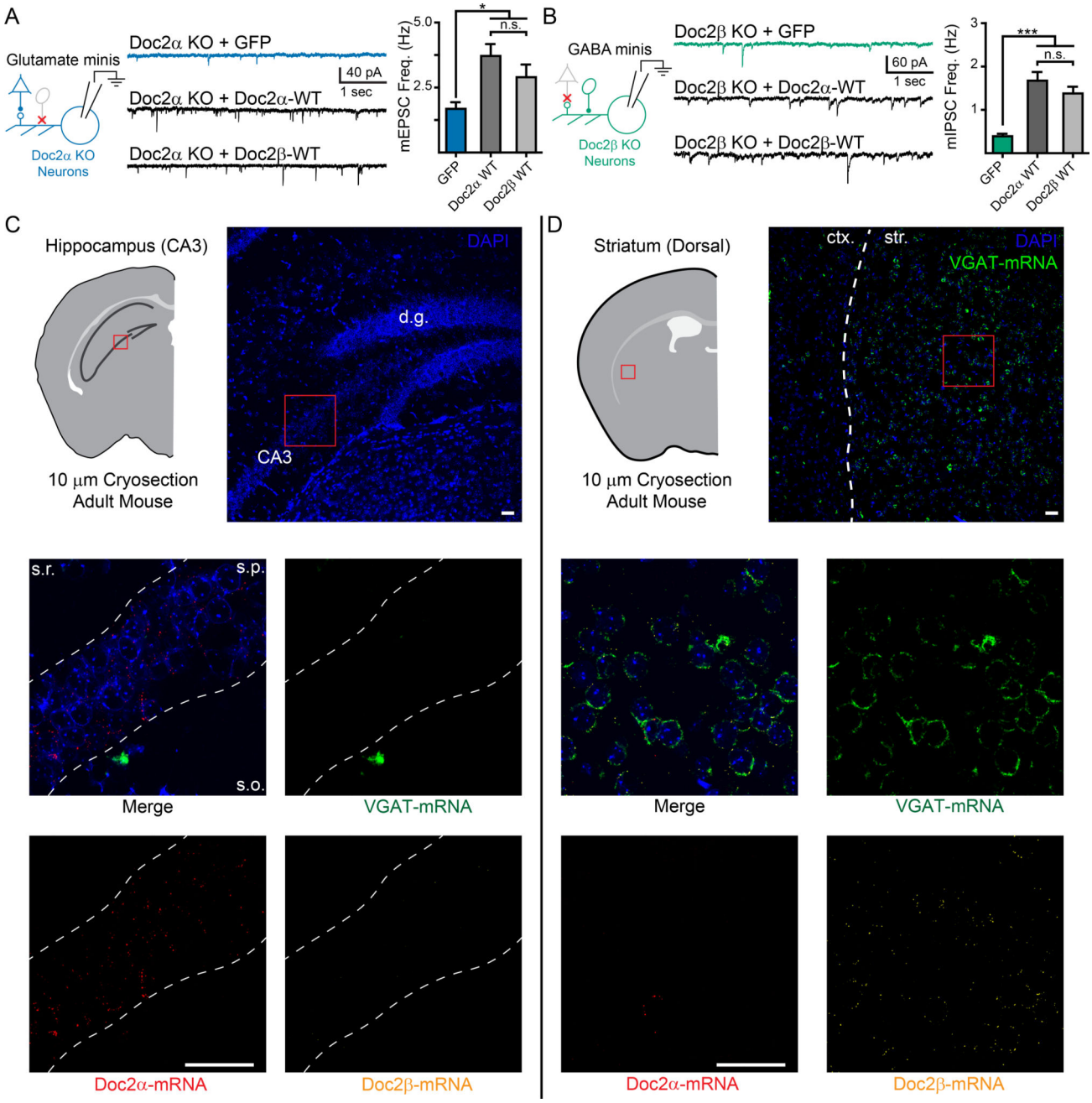


**Figure 5.**

Doc2α and β are functionally redundant but differentially expressed in excitatory and inhibitory neurons. **A.** Representative traces (center) and quantification (right) demonstrating that neuronal, non-subtype specific expression of Doc2β WT rescues mEPSC frequency in Doc2α single KO neurons (left). **B.** Representative traces (center) and quantification (right) demonstrating that neuronal, non-subtype specific expression of Doc2α WT rescues mIPSC frequency in Doc2β single KO neurons (left). Note, the experiments presented in panels A and B were performed in parallel to those in Fig. 4B and D, respectively. Thus, the data for GFP controls, Doc2α WT in *panel (A)*, and Doc2β WT in *panel (B)*, are reproduced here

from those previous figures to facilitate comparisons. **C** and **D.** RNAScope images examining the cellular distribution of Doc2 isoforms in glutamatergic CA3 pyramidal neurons in the hippocampus (**C**) and GABAergic neurons in the striatum (**D**) visualized in coronal brain slices (10 μM thick) obtained from adult mice. *Upper*. Cartoon representation and low-magnification images demonstrating gross morphology of the brain slices imaged. Abbreviations: d.g. = dentate gyrus, ctx. = cortex, and str. = striatum. Red boxes approximate the regions examined in the lower panels, but do not directly correlate. *Middle and lower*. High-magnification images showing the distribution of Doc2α-mRNA (red), Doc2β-mRNA (yellow), and VGAT-mRNA (green) among neurons (indicated by DAPI, blue). Abbreviations: s.r. = stratum radiatum, s.p. = stratum pyramidale, and s.o. = stratum oriens. Scale bars (white) represent 50 μm and apply to all lower panels. Images were adjusted for brightness/contrast; corresponding channels underwent the exact same adjustments. RNAScope experiments were performed three times, on separate animals, and similar results were observed each time. White dashed lines were overlaid on the images to help highlight morphology. *** indicates $p < 0.001$, * indicates $p < 0.05$, and n.s. indicates $p > 0.05$. Bar graphs represent mean ± SEM.

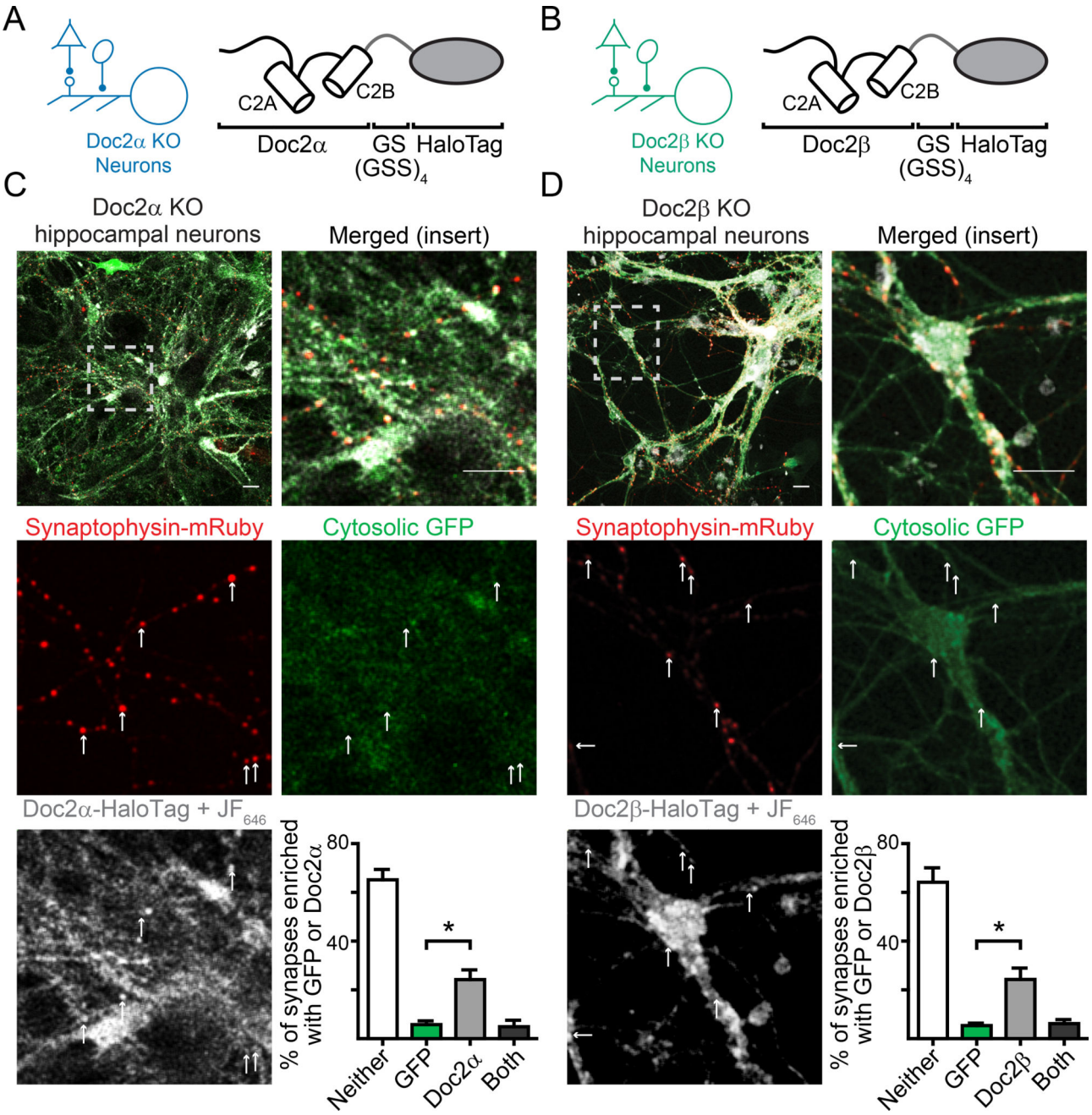


**Figure 6.**

Doc2 isoforms are enriched at synaptic boutons. **A**. Schematic demonstrating the fusion of HaloTag to Doc2α and (**B**) Doc2β. **C.** Representative live cell confocal images demonstrating that Doc2α-HaloTag (white), expressed at low levels in Doc2α KO neurons, is enriched in synaptic compartments identified by the presence of mRuby-tagged synaptophysin (red). Neurons were co-infected with virus expressing soluble GFP (green), which was not enriched in synapses. The JF646 dye was used because it is significantly brighter than protein fluorophores and fluoresces only when bound to HaloTag proteins *Upper-right*: quantification of percentage of synaptophysin-positive boutons (synapses) that

had punctate enrichment of GFP or Doc2α. **D.** Similar to C, Doc2β-HaloTag (white) also is enriched in synaptic compartments when expressed in Doc2β KO neurons. * denotes $p < 0.05$, ** denotes $p < 0.01$, *** denotes $p < 0.001$, n.s. denotes $p > 0.05$. Scale bar represents 20 μm. Bar graphs represent mean ± SEM. See also Supp. Fig. 5 and 6.

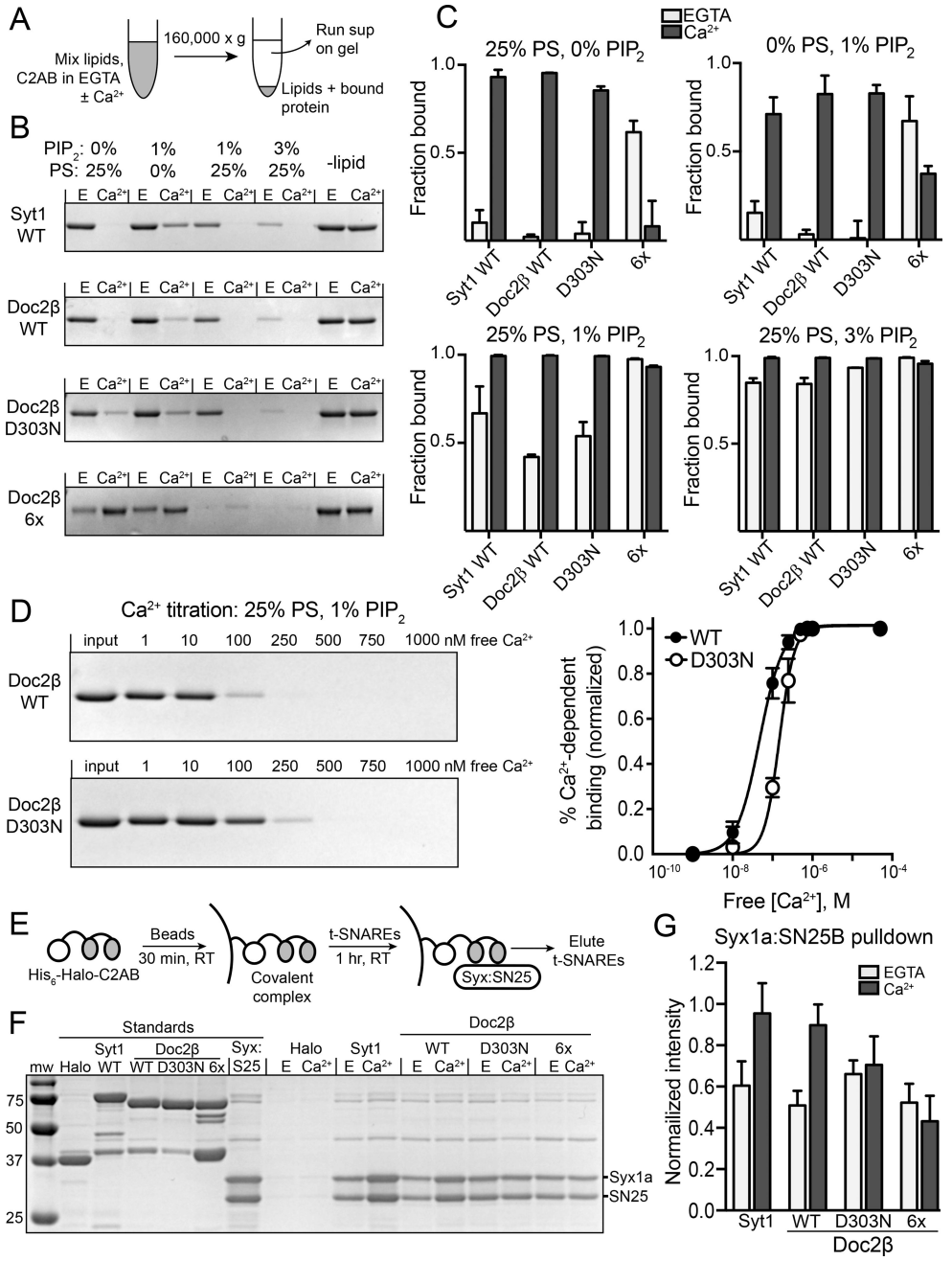


**Figure 7.**

$Ca^{2+}$-dependent and –independent interactions of WT and mutant forms of Doc2β with t-SNAREs and phospholipids. **A.** Scheme of cosedimentation assay. **B**. Representative images of Coomassie-stained gels from a cosedimentation assay varying liposome composition. Disappearance of the band signifies depletion of the supernatant due to protein-liposome interactions. **C**. Quantification of C2AB-liposome cosedimentation in varying lipid compositions ($n$ = 2–3 independent experiments). In syt1 WT, Doc2β WT, and Doc2β D303N, $Ca^{2+}$-independent binding is minimal with liposomes containing either PS or $PIP_2$ but increases when both phospholipids are present. Doc2β 6x exhibits substantially greater

$Ca^{2+}$-independent binding to both $PIP_2$ and PS. **D**. Representative gel and quantification of cosedimentation performed while titrating free $Ca^{2+}$ ($n = 4$ independent experiments). Apparent $[Ca^{2+}]_{1/2}$ values and Hill slopes were: WT: 47.3 ± 5.1 nM, $n = 1.49 \pm 0$-.16; D303N: 148 ± 12 nM, $n = 2.30 \pm 0.38$. **E**. Scheme of HaloTag-based pulldown assay. t-SNARES were eluted in SDS sample buffer. **F**. Representative gel from HaloTag pulldown assay. Only the bound heterodimer is eluted, as the HaloTag-C2AB fusion construct remains bound to the beads. The unlabeled bands (~40 and ~75 kD) are trace contaminants associated with the t-SNARE heterodimer preparation. **G.** Eluted t-SNAREs were quantified from pulldown assays ($n = 5$) via normalization to t-SNARE loading control. $Ca^{2+}$-independent binding was similar among all constructs, with only WT Syt1 and Doc2β demonstrating $Ca^{2+}$-dependent increases in SNARE binding. Bar graphs represent mean ± SEM.

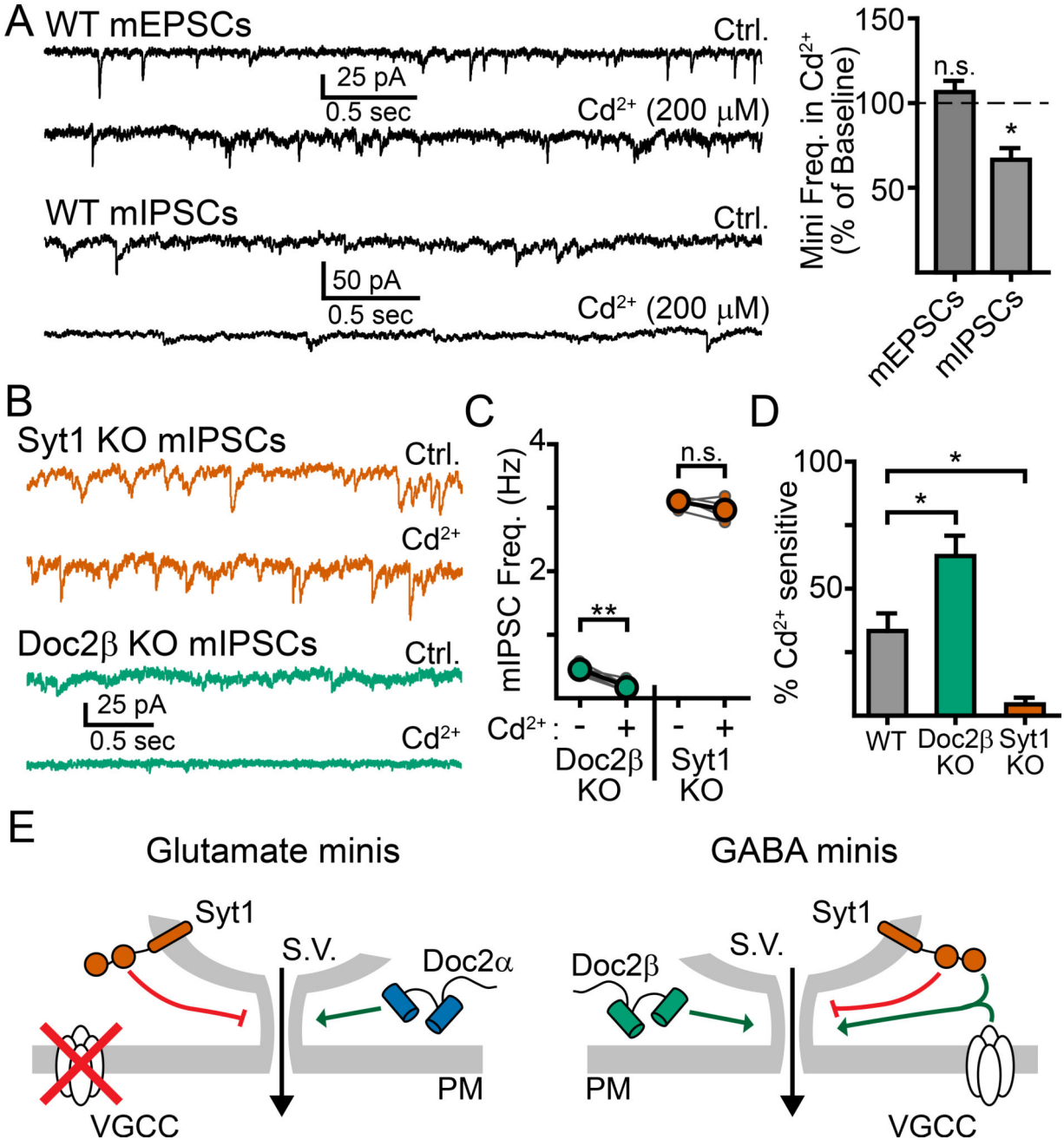


**Figure 8.**

$Ca^{2+}$-influx via VGCCs activates syt1 to drive spontaneous GABA, but not glutamate, release. **A.** Example traces (left) and quantification (right) demonstrating that the non-specific voltage-gated $Ca^{2+}$ channel blocker cadmium ($Cd^{2+}$, 200 μM) reduced the frequency of mIPSCs but not mEPSCs. **B.** Representative traces and quantification (**C**) comparing the effects of $Cd^{2+}$ on mIPSCs in syt1 and Doc2β KO cultures. Recordings were made first in control conditions before adding $Cd^{2+}$ to the bath. Then, the same cell was recorded again in $Cd^{2+}$; each pair of recordings is depicted with small connected circles, with the overall average shown as larger, bold, circles. **D.** Quantification of the percentage of

mIPSCs that were sensitive to $Cd^{2+}$. Whereas $Cd^{2+}$ had a substantially larger effect in Doc2β KO neurons, this inhibitory effect was absent in syt1 KO neurons. **E.** Cartoon schematic depicting possible $Ca^{2+}$-dependent pathways leading to spontaneous neurotransmission in excitatory (left) and inhibitory (right) neurons. * denotes $p < 0.05$, ** denotes $p < 0.01$, *** denotes $p < 0.001$, n.s. denotes $p > 0.05$. Bar graphs represent mean ± SEM.